J. Fluid Mech. (1992), *vol.* 235, *pp.* 579–609
Printed in Great Britain

Viscous oscillations of capillary bridges

By JOHN TSAMOPOULOS†, TAY-YUAN CHEN AND ABHAY BORKAR

Department of Chemical Engineering, State University of New York at Buffalo, Buffalo, NY 14260, USA

(Received 15 March 1991)

Small-amplitude oscillations of viscous, capillary bridges are characterized by their frequency and rate of damping. In turn, these depend on the surface tension and viscosity of the liquid, the dimensions of the bridge, the axial and azimuthal wavenumbers of each excited mode and the relative magnitude of gravity. Both analytical and numerical methods have been employed in studying these effects. Increasing the gravitational Bond number decreases the eigenvalues in addition to modifying the well-known Rayleigh stability limit for meniscus breakup. At high Reynolds numbers results from inviscid and boundary-layer theories are recovered. At very low Reynolds numbers oscillations become overdamped. The analysis is applicable in measuring properties of semiconductor and ceramic materials at high temperatures under well-controlled conditions. Such data are quite scarce.

1. Introduction

Static shapes and stability of a fluid mass placed between two solid surfaces and in the presence or absence of a gravitational field have been studied since the original work by Plateau (1863). Rayleigh (1879) has shown that fluid masses of cylindrical shape become unstable when the ratio of their length ($\tilde{L}$) to radius ($\tilde{R}$) exceeds 2π. Under these conditions, small sinusoidal perturbations of wavelength $2\pi\tilde{R}$ have less surface area than the cylinder of the same volume and capillary forces make the latter unstable. When gravity is present, instability arises even for smaller values of $\tilde{L}$. These values depend on the relative magnitude of surface tension and gravitational forces, i.e. the gravitational Bond number (Coriell, Hardy & Cordes 1977). Various aspects of the static problem have been reported; see, for example, Russo & Steen (1986).

There is renewed interest in the stability limit as well as the dynamics of liquid bridges owing to their employment in fabricating single semiconductor crystals of high purity from the melt according to the floating zone method (Brown 1988). In this process, resistive heating is used to form a molten bridge between a melting polycrystalline feed rod and a solidifying cylindrical crystal. Buoyancy-driven convection and capillary instabilities in the bridge are inevitable in the presence of gravity. Thus, crystals may be grown with conventional heaters, but their diameters are limited to less than about 1 cm. This limitation is reduced considerably in a gravity-free environment. Even in space, the floating zone is susceptible to dynamic disturbances since it possesses a free liquid/gas interface. These may result from g-jitter, spacecraft manoeuvers and vibration of machines on board and may excite

† Author to whom correspondence should be addressed.

oscillations of the free interface. Consequently, it is important to know the natural frequencies and decay rates of the zone after such disturbances.

In a different context, a floating zone has been proposed as a convenient system for simultaneously measuring surface tension and viscosity of ceramic materials at high temperatures (1000–3000 °C). Existing data are extremely limited and somewhat unreliable. Currently available methods cannot be employed at these high temperatures or data produced are adversely affected by contamination of materials through contact with the apparatus used (Lihrmann & Haggerty 1985; Finucane & Olander 1969). In contrast to this, aluminium oxides, for example, may be melted and heated up to the desired temperature using a CO_2 laser beam. A carefully controlled axial excitation of the liquid zone will result in longitudinal capillary waves on the cylindrical surface which may be over- or underdamped. It is anticipated that the damping rate and oscillation frequency are directly related to surface tension and viscosity of the material, at that temperature.

Certain preliminary experiments and analysis of the dynamics of a liquid zone have been performed by Fowle, Wang & Strong (1979). They used an experimental set-up similar to Plateau's and water as the liquid in the zone. Their analysis is confined to either solid-body rotation or inviscid oscillation. The latter is adequate for water which, owing to its high surface tension (in the absence of contamination) and low viscosity, exhibits very small damping. However, this is not the case for most other materials, including either molten semiconductors or ceramics. Inviscid analysis in zero gravity has been performed also by Sanz (1985) and Sanz & Diez (1989) among others. They considered the effects of a liquid surrounding the bridge and of non-axisymmetric disturbances. Such an analysis cannot predict the damping rate of the oscillations and will have to allow for a slip velocity at the solid/liquid and liquid/liquid interfaces; see figure 8 in Sanz (1985).

As an alternative method for measuring surface tension and viscosity of various materials, Trinh, Zwern & Wang (1982) and Trinh, Marston & Robey (1988) have proposed studying the oscillations of acoustically levitated drops. Sound waves are used to position the drop in an immiscible fluid as well as to excite the oscillations. To account for small discrepancies from linear theory, the same authors have mentioned the drawbacks of this technique, namely (1) the levitation mechanism produces static drops that are not perfect spheres; (2) non-axisymmetric oscillations, translation and rotation of the drops may be inadvertently induced within the acoustic well; (3) usually, nonlinear effects are present.

Several theoretical aspects of the oscillations of viscous drops have been studied since the original work of Chandrasekhar (1959). For example, Miller & Scriven (1968) analysed the linear modes of viscous drops immersed in another immiscible fluid and examined several limiting cases. They have shown that viscous boundary layers are formed on both sides of the liquid/liquid interface. Thus, viscous dissipation is induced, even when the viscosities of both fluids are small. Prosperetti (1980) and Basaran, Scott & Byers (1989) have presented numerical solutions to the corrected form of the dispersion relation calculated by Miller & Scriven. Strani & Sabetta (1988) examined the effect of a solid support under the oscillating drop. In an effort to explain observations by Trinh *et al.* (1982) related to large-amplitude oscillations, Tsamopoulos & Brown (1983) performed a weakly nonlinear analysis of inviscid oscillations.

These investigations of drop vibrations immersed in another fluid are not suitable for crystal growth problems where the drop cannot be considered to be isolated. Moreover, experiments with acoustically levitated drops have the above-mentioned

shortcomings for measuring material properties. All these have prompted investigating the normal modes of liquid bridges. A boundary-layer analysis which is valid for fluids with large modified Reynolds numbers (Borkar & Tsamopoulos 1991) was followed by the present analysis, which is valid for arbitrary Re and delineates the limits of applicability of the former.

The governing equations for both gravity and gravity-free cases are given in §2. These equations are linearized and the eigenvalue problem is formulated in §3. An analytical solution for axisymmetric disturbances in zero gravity is presented in §4. It is based on the separation of variables methodology for the biharmonic equation which was given first by Smith (1952). In contrast to the normal mode analysis for either drop oscillations or liquid columns free from contact with solid boundaries, where the analysis is comparatively straightforward, it is found that each mode of the present system involves an infinite summation. This leads to a complicated eigenvalue problem which requires extensive computational effort for its accurate solution. These semi-analytic results are used as a starting and testing point for the more extensive numerical ones that follow. To this end, the finite-element technique is employed in §5 in order to reduce the differential eigenvalue problem to a generalized algebraic eigenvalue problem. Results and discussion follow in §6 and conclusions are drawn in §7.

The present analysis has proven most valuable in undertaking numerical solutions of the full nonlinear problem and experiments. The former are computationally very expensive and time-consuming and they would be even more so in the absence of results presented here. The latter may proceed as follows. The surface tension of the fluid may be measured first by a static method. Experimental shapes of bridges or pendant drops are matched with calculated ones for various Bond numbers B. Knowledge of the fluid volume and gravitational acceleration will yield the surface tension (Padday 1971; Lihrmann & Haggerty 1985; Tsamopoulos, Poslinski & Ryan 1988). Then, the present dynamic method may be used for viscosity measurements. Alternatively, only the dynamic method may be used to experimentally measure resonance frequencies. Then the external forcing is removed and the damping rate is also measured. Figures and data provided herein and in Chen (1991) are used to calculate Re and B and, thus, surface tension and viscosity of the fluid.

2. Governing equations

A nearly cylindrical liquid bridge of volume $\tilde{V}$ is considered. As shown in figure 1, the bridge is situated between two stationary, solid and coaxial rods of equal radius $\tilde{R}$. The liquid wets the two planar surfaces which are at a distance $\tilde{L}$ from each other and forms a fixed and circular contact line on the edge of each one. It is assumed that the surrounding gas has negligible density and viscosity so that it does not affect the dynamics of the liquid bridge. Furthermore, bulk properties (density ρ and viscosity μ) as well as interfacial properties (surface tension γ) of the liquid are uniform and constant under the present isothermal analysis.

This shape of the liquid bridge is sustained by capillary forces as long as the Plateau stability limit is not exceeded. Small disturbances may initiate motion of the liquid, which can be easily detected at the side surface. This motion is affected by the physical properties of the liquid and its static shape, which in turn depends on $\tilde{R}$, $\tilde{L}$ and gravity. Gravity acts downwards along the z-axis. The usual cylindrical coordinate system (r, θ, z) with origin midway between the two solids and coaxial with them is defined. The corresponding components of velocity are $\boldsymbol{v} = (u, v, w)$. The

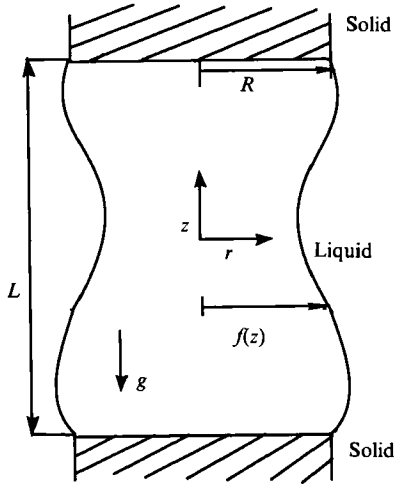

FIGURE 1. Schematic representation of a liquid bridge.

goal is to calculate the eigenfrequencies and eigenmodes and relate them to the physical properties of this system. To this end, conservation equations of mass and momentum are written in dimensionless form:

$$\nabla \cdot \boldsymbol{v} = 0, \tag{2.1}$$

$$Re\left(\frac{\partial \boldsymbol{v}}{\partial t} + \boldsymbol{v} \cdot \nabla \boldsymbol{v}\right) = -Re\,\nabla \mathscr{P} + \nabla \cdot \boldsymbol{\tau}, \tag{2.2}$$

where the modified pressure is defined by $\mathscr{P} = P - Bz$ (Batchelor 1967) and the extra stress tensor is defined by $\boldsymbol{\tau} = [\nabla \boldsymbol{v} + (\nabla \boldsymbol{v})^{\mathrm{T}}]$. Variables have been rendered dimensionless with respect to their dimensional counterparts as follows:

$$z = \tilde{z}\frac{\pi}{\tilde{L}}, \quad r = \frac{\tilde{r}}{\tilde{R}}, \quad P = \tilde{P}\frac{\tilde{R}}{\gamma}, \quad \boldsymbol{v} = \tilde{\boldsymbol{v}}\left(\frac{\rho\tilde{R}}{\gamma}\right)^{\frac{1}{2}}, \quad t = \tilde{t}\left(\frac{\gamma}{\rho\tilde{R}^3}\right)^{\frac{1}{2}}.$$

As a result, the gravitational Bond number $B = \rho g \tilde{R}\tilde{L}/\pi\gamma$ (g is the gravitational acceleration) and the modified Reynolds number, $Re = (\rho\gamma\tilde{R})^{\frac{1}{2}}/\mu$ arise in (2.2). Since there is no characteristic velocity in this problem, only physical and geometrical properties appear in what is called the modified Re. The same group of parameters is sometimes referred to as the Suratman number, $Su = \rho\gamma\tilde{R}/\mu^2$, or the Ohnesorge number, $Oh = \mu/(\rho\gamma\tilde{R})^{\frac{1}{2}}$. Different lengthscales have been used in the radial and axial directions and their ratio, $\Lambda = \pi\tilde{R}/\tilde{L}$, is the third dimensionless parameter of this system. It arises, for example, in the dimensionless form of the gradient operator:

$$\nabla = \boldsymbol{e}_r\frac{\partial}{\partial r} + \boldsymbol{e}_\theta\frac{1}{r}\frac{\partial}{\partial \theta} + \boldsymbol{e}_z\Lambda\frac{\partial}{\partial z}. \tag{2.3}$$

The usual no-slip and no-penetration boundary conditions apply at both solid surfaces

$$\boldsymbol{v} = 0, \quad z = \pm\tfrac{1}{2}\pi. \tag{2.4}$$

When axisymmetric disturbances are considered, the azimuthal velocity is zero

throughout the bridge and the radial velocity and its derivative with respect to r are zero at the centreline. Combining this fact with (2.1) and (2.4) shows that the axial velocity also must be zero at the centreline. Therefore

$$u = \frac{\partial u}{\partial r} = v = w = 0, \quad r = 0. \tag{2.5a}$$

When non-axisymmetric disturbances are considered, the axial velocity at the centreline must remain independent of θ, which can only be satisfied if it is equal to zero. The condition on the radial and azimuthal velocities depends on the wavenumber, k, of the disturbance in the azimuthal direction (Preziosi, Chen & Joseph 1989):

$$k = 1: \quad u + v = w = 0, \quad r = 0, \tag{2.5b}$$

$$k \geqslant 2: \quad u = v = w = 0, \quad r = 0. \tag{2.5c}$$

Moreover, at the liquid/gas interface the tangential stresses must be zero and the total normal stress must be balanced by the capillary force:

$$\boldsymbol{t}_\theta \cdot \boldsymbol{\tau} = \boldsymbol{t}_z \cdot \boldsymbol{\tau} = 0, \quad r = f(\theta, z, t), \tag{2.6}$$

$$[Re(-P + Bz)\boldsymbol{I} + \boldsymbol{\tau}] \cdot \boldsymbol{N} + Re\, 2\mathscr{H}\boldsymbol{N} = 0, \quad r = f(\theta, z, t). \tag{2.7}$$

In (2.6) and (2.7) the ambient pressure has been taken as the reference pressure and $\boldsymbol{t}_\theta$, $\boldsymbol{t}_z$ and $\boldsymbol{N}$ are the unit tangents and outward-pointing normal to the interface, respectively. In the Mongé representation, a point on this interface can be described by the position vector $\boldsymbol{F}(\theta, z, t) = f(\theta, z, t)\,\boldsymbol{e}_r + z\boldsymbol{e}_z$; consequently, $\boldsymbol{N}$ is given by

$$\boldsymbol{N} = \frac{f\boldsymbol{e}_r - f_\theta \boldsymbol{e}_\theta - \Lambda f f_z \boldsymbol{e}_z}{(f^2 + f_\theta^2 + \Lambda^2 f^2 f_z^2)^{\frac{1}{2}}}, \tag{2.8}$$

where the subscripts z and θ denote partial differentiation with respect to that coordinate. Specific expressions for the tangent vectors will be given in the next section. The curvature of this interface, $2\mathscr{H}$, has been scaled by $\tilde{R}^{-1}$ and is equal to

$$2\mathscr{H} = \frac{1}{f}\left[\frac{f(1 + \Lambda^2 f_z^2)}{D^{\frac{1}{2}}} - \frac{\partial}{\partial\theta}\left(\frac{f_\theta}{D^{\frac{1}{2}}}\right) - \Lambda^2 \frac{\partial}{\partial z}\left(\frac{f^2 f_z}{D^{\frac{1}{2}}}\right)\right], \tag{2.9}$$

where $D = f^2 + f_\theta^2 + \Lambda^2 f^2 f_z^2$, see, for example, Tsamopoulos *et al.* (1988).

Another boundary condition that arises at the moving interface is the kinematic condition. It equates the velocity of the surface to the fluid velocity there:

$$\boldsymbol{N} \cdot \frac{\partial \boldsymbol{F}}{\partial t} = \boldsymbol{N} \cdot \boldsymbol{v}, \quad r = f(\theta, z, t). \tag{2.10}$$

Throughout the motion, the line of contact of the liquid/gas interface with each cylindrical rod remains fixed at the edge of each rod. According to the analysis by Benjamin & Scott (1979), this is the relevant condition, especially when a sharp corner is present in the supporting solid surface. Thus,

$$f(\theta, t) = 1, \quad z = \pm\tfrac{1}{2}\pi. \tag{2.11}$$

Moreover, all velocity components and the liquid/gas interface must be periodic in the azimuthal direction with periodicity 2π:

$$f(\theta, z, t) = f(\theta + 2\pi, z, t). \tag{2.12}$$

Finally, the volume of the liquid bridge must remain constant during the motion. Although other cases may be readily examined, volume is taken here to be equal to the volume of the space between the rods:

$$V \equiv \frac{\tilde{V}}{\tilde{R}^2\tilde{L}} = \frac{1}{2\pi}\int_0^{2\pi}\int_{-\pi/2}^{\pi/2} f^2\,\mathrm{d}z\,\mathrm{d}\theta = \pi. \tag{2.13}$$

3. Basic state and the eigenvalue problem

In order to calculate the eigenvalues and eigenmodes of this system all equations will be linearized around a steady state. To this end, small and volume-preserving disturbances of amplitude ϵ will be assumed for all dependent variables. Thus,

$$\boldsymbol{v} = \boldsymbol{v}_\mathrm{b} + \epsilon\boldsymbol{v}_\mathrm{p}, \quad P = P_\mathrm{b} + \epsilon P_\mathrm{p}, \quad f = f_\mathrm{b} + \epsilon f_\mathrm{p}, \quad \boldsymbol{\tau} = \boldsymbol{\tau}_\mathrm{b} + \epsilon\boldsymbol{\tau}_\mathrm{p}, \tag{3.1}$$

where the subscript b indicates the base, static state and the subscript p indicates the perturbed one. Therefore, $\boldsymbol{\tau}_\mathrm{b} = \boldsymbol{0}, \boldsymbol{v}_\mathrm{b} = \boldsymbol{0}, P_\mathrm{b}$ is the hydrostatic pressure, and f_b is the static shape. If gravity effects are negligible, $P_\mathrm{b} = 1$ and $f_\mathrm{b} = 1$. On the other hand, if the gravitational Bond number is not zero, $P_\mathrm{b} \neq 1$ and f_b is a function of the axial distance. Both are calculated by solving the hydrostatic problem:

$$-P_\mathrm{b} + Bz + 2\mathscr{H}_\mathrm{b} = 0, \tag{3.2}$$

$$f_\mathrm{b}(z = \pm\tfrac{1}{2}\pi) = 1, \tag{3.3}$$

$$\int_{-\pi/2}^{\pi/2} f_\mathrm{b}^2\,\mathrm{d}z = \pi. \tag{3.4}$$

Since gravity acts along the common z-axis of the cylindrical rods, there will be no θ-dependence on the base shape, so that

$$2\mathscr{H}_\mathrm{b} = \frac{1}{f_\mathrm{b}}\left[D_\mathrm{b}^{\frac{1}{2}} - A^2\frac{\partial}{\partial z}\left(\frac{f_\mathrm{b}}{D_\mathrm{b}^{\frac{1}{2}}}\frac{\partial f_\mathrm{b}}{\partial z}\right)\right], \tag{3.5}$$

and $D_\mathrm{b} = 1 + A^2(\partial f_\mathrm{b}/\partial z)^2$. Introducing (3.1) into the governing equations of the previous section results in a set of equations for the perturbed variables:

$$\boldsymbol{\nabla}\cdot\boldsymbol{v}_\mathrm{p} = 0, \tag{3.6}$$

$$Re\frac{\partial \boldsymbol{v}_\mathrm{p}}{\partial t} = -Re\,\boldsymbol{\nabla}P_\mathrm{p} + \boldsymbol{\nabla}\cdot\boldsymbol{\tau}_\mathrm{p}, \tag{3.7}$$

$$\boldsymbol{v}_\mathrm{p} = \boldsymbol{0}, \quad z = \pm\tfrac{1}{2}\pi, \tag{3.8}$$

$$u_\mathrm{p} = v_\mathrm{p} = w_\mathrm{p} = 0, \quad r = 0, \quad k = 0, 2, 3, 4, \ldots, \tag{3.9a}$$

$$u_\mathrm{p} + v_\mathrm{p} = w_\mathrm{p} = 0, \quad r = 0, \quad k = 1, \tag{3.9b}$$

$$\boldsymbol{t}_{\theta,\mathrm{b}}\cdot\boldsymbol{\tau}_\mathrm{p} = \boldsymbol{t}_{z,\mathrm{b}}\cdot\boldsymbol{\tau}_\mathrm{p} = \boldsymbol{0}, \quad r = f_\mathrm{b}(z), \tag{3.10}$$

$$(-Re\,P_\mathrm{p}\boldsymbol{I} + \boldsymbol{\tau}_\mathrm{p})\cdot\boldsymbol{N}_\mathrm{b} + Re\,2\mathscr{H}_\mathrm{p}\boldsymbol{N}_\mathrm{b} = 0, \quad r = f_\mathrm{b}(z), \tag{3.11}$$

$$\boldsymbol{N}_\mathrm{b}\cdot\boldsymbol{e}_r\frac{\partial f_\mathrm{p}}{\partial t} = \boldsymbol{N}_\mathrm{b}\cdot\boldsymbol{v}_\mathrm{p}, \quad r = f_\mathrm{b}(z), \tag{3.12}$$

$$f_\mathrm{p} = 0 \quad \text{at} \quad z = \pm\tfrac{1}{2}\pi, \qquad \int_{-\pi/2}^{\pi/2} f_\mathrm{p}\,\mathrm{d}z = 0, \tag{3.13a, b}$$

$$f_\mathrm{p}(\theta, z, t) = f_\mathrm{p}(\theta + 2\pi, z, t). \tag{3.14}$$

In the equations above

$$N_b = \frac{e_r - A(\partial f_b/\partial z)\, e_z}{D_b^{\frac{1}{2}}}, \quad t_{\theta,b} = e_\theta, \quad t_{z,b} = \frac{A(\partial f_b/\partial z)\, e_r + e_z}{D_b^{\frac{1}{2}}}. \tag{3.15}$$

When $B = 0$, (3.5) and (3.15) reduce to $2\mathscr{H}_b = 1$, $N_b = e_r$, and $t_{z,b} = e_z$. The perturbed form of the surface curvature is the first-order term in a Taylor series expansion of $2\mathscr{H}$ around its base state. In the absence of gravity and for general three-dimensional disturbances

$$2\mathscr{H}_p = -f_p - \frac{\partial^2 f_p}{\partial \theta^2} - A^2 \frac{\partial^2 f_p}{\partial z^2}. \tag{3.16}$$

When gravitational effects are accounted for, but only two-dimensional disturbances are considered

$$2\mathscr{H}_p = -\frac{1}{f_b^2 D_b^{\frac{1}{2}}} f_p - \frac{A^2(\partial f_b/\partial z)}{f_b D_b^{\frac{3}{2}}} \frac{\partial f_p}{\partial z} + \frac{3A^4(\partial f_b/\partial z)(\partial^2 f_b/\partial z^2)}{D_b^{\frac{5}{2}}} \frac{\partial f_p}{\partial z} - \frac{A^2}{D_b^{\frac{3}{2}}} \frac{\partial^2 f_p}{\partial z^2}. \tag{3.17}$$

Finally, according to the usual normal mode methodology all perturbed variables are decomposed as

$$\left.\begin{aligned} u_p(r,\theta,z,t) = \hat{u}(r,z)\, e^{ik\theta} e^{-\sigma t}, \quad v_p(r,\theta,z,t) = i\hat{v}(r,z)\, e^{ik\theta} e^{-\sigma t}, \\ w_p(r,\theta,z,t) = \hat{w}(r,z)\, e^{ik\theta} e^{-\sigma t}, \\ P_p(r,\theta,z,t) = \hat{P}(r,z)\, e^{ik\theta} e^{-\sigma t}, \quad f_p(\theta,z,t) = \hat{f}(z)\, e^{ik\theta} e^{-\sigma t}, \end{aligned}\right\} \tag{3.18}$$

where k is the wavenumber in the azimuthal direction and σ is the eigenvalue of the system which is complex in general, $\sigma = \sigma_r + i\sigma_i$. After introducing (3.18) into the equations for the perturbed variables, an equation set is obtained that is similar to the above one except for two substitutions: $\partial(\,)/\partial t \to -\sigma(\,)$, $\partial(\,)/\partial\theta \to ik(\,)$.

Typically, a distinct eigenvalue corresponds to each eigenmode. If the real part of all eigenvalues is positive, the system is linearly stable, and the distinct values of σ_r and σ_i correspond to the damping rate and frequency of each mode, respectively. On the other hand, if the real part of even one eigenvalue is negative the system is unstable. Clearly the values of σ depend on the parameters of the system (Re, B, A, k). In physical space, the point at which $\sigma_r = 0$ is called a bifurcation point.

4. Analytical solution for axisymmetric disturbances in zero gravity ($B = k = 0$)

In the absence of gravity ($B = 0$) and when only axisymmetric disturbances are considered ($k = 0$), introducing the stream function, ψ, facilitates the analysis. The usual definition of the stream function,

$$\frac{\partial \psi}{\partial r} \equiv -r\hat{w}, \frac{\partial \psi}{\partial z} \equiv +r\hat{u}, \tag{4.1}$$

reduces (3.7) to

$$\left(L^2 + \frac{Re}{A}\sigma\right) L^2 \psi = 0, \tag{4.2}$$

where

$$L^2 = A\frac{\partial^2}{\partial z^2} + \frac{1}{A}\left(\frac{\partial^2}{\partial r^2} - \frac{1}{r}\frac{\partial}{\partial r}\right).$$

This equation must be solved subject to the following conditions:

$$\psi = \frac{\partial \psi}{\partial z} = 0, \quad z = \pm \tfrac{1}{2}\pi, \tag{4.3}$$

$$\psi = \frac{\partial}{\partial r}\left(\frac{1}{r}\frac{\partial \psi}{\partial r}\right) = 0, \quad r = 0, \tag{4.4}$$

$$\frac{\Lambda^2}{r}\frac{\partial^2 \psi}{\partial z^2} - \frac{\partial}{\partial r}\left(\frac{1}{r}\frac{\partial \psi}{\partial r}\right) = 0, \quad r = 1, \tag{4.5}$$

$$-\hat{P} + 2\frac{1}{Re}\frac{\partial}{\partial r}\left(\frac{1}{r}\frac{\partial \psi}{\partial z}\right) = \Lambda^2 \frac{\partial^2 \hat{f}}{\partial z^2} + \hat{f}, \quad r = 1, \tag{4.6}$$

$$\frac{\partial \psi}{\partial z} = -\sigma \hat{f}, \quad r = 1. \tag{4.7}$$

Equations (4.3)–(4.7) result from inserting definition (4.1) in (3.8)–(3.12) of the previous section. A general solution for ψ can be found by separation of variables. The methodology in a simpler setting is given in the original work by Smith (1952) and has been applied by Joseph and co-workers in several problems (e.g. Yoo & Joseph 1978; Joseph, Sturges & Warner 1982). However, the current physical problem is time-dependent and in addition periodicity in the axial direction cannot be invoked. Therefore, a different eigenvalue problem must be solved. Very briefly, the even-mode solution to (4.2) subject to conditions (4.3) and (4.4) is

$$\psi_e(r, z) = \sum_{n=0}^{\infty} C_{en} Z_{en}(z)\, r I_1(\alpha_{2n} \Lambda r), \tag{4.8}$$

and the odd-mode solution is

$$\psi_o(r, z) = \sum_{n=0}^{\infty} C_{on} Z_{on}(z)\, r I_1(\beta_{2n} \Lambda r), \tag{4.9}$$

where I_1 is the modified Bessel function of the first kind and of order one. Also, $Z_{en}(z)$ is the solution to the following eigenvalue problem:

$$\frac{\mathrm{d}^2}{\mathrm{d}z^2}\begin{bmatrix} Z_{en} \\ Z_{en}^* \end{bmatrix} = \begin{bmatrix} 0 & \alpha_{2n}^2 \\ -\alpha_{1n}^2 & -(\alpha_{1n}^2 + \alpha_{2n}^2) \end{bmatrix}\begin{bmatrix} Z_{en} \\ Z_{en}^* \end{bmatrix}, \tag{4.10}$$

$$Z_{en} = \frac{\mathrm{d}Z_{en}}{\mathrm{d}z} = 0, \quad z = \pm \tfrac{1}{2}\pi, \tag{4.11}$$

so that

$$Z_{en} = \cos(\alpha_{1n} z) - \frac{\cos(\alpha_{1n} \tfrac{1}{2}\pi)}{\cos(\alpha_{2n} \tfrac{1}{2}\pi)} \cos(\alpha_{2n} z), \tag{4.12}$$

and the eigenvalues are given by

$$\alpha_{1n} \tan(\alpha_{1n} \tfrac{1}{2}\pi) = \alpha_{2n} \tan(\alpha_{2n} \tfrac{1}{2}\pi), \quad \alpha_{1n} = \left(\alpha_{2n}^2 + \frac{Re\,\sigma}{\Lambda^2}\right)^{\frac{1}{2}}. \tag{4.13}$$

Similarly, $Z_{on}(z)$ is the solution to the following eigenvalue problem:

$$\frac{\mathrm{d}^2}{\mathrm{d}z^2}\begin{bmatrix} Z_{on} \\ Z_{on}^* \end{bmatrix} = \begin{bmatrix} 0 & \beta_{2n}^2 \\ -\beta_{1n}^2 & -(\beta_{1n}^2 + \beta_{2n}^2) \end{bmatrix}\begin{bmatrix} Z_{on} \\ Z_{on}^* \end{bmatrix}, \tag{4.14}$$

$$Z_{on} = \frac{\mathrm{d}Z_{on}}{\mathrm{d}z} = 0, \quad z = \pm\tfrac{1}{2}\pi, \tag{4.15}$$

so that

$$Z_{on} = \sin(\beta_{1n} Z) - \frac{\sin(\beta_{1n}\tfrac{1}{2}\pi)}{\sin(\beta_{2n}\tfrac{1}{2}\pi)}\sin(\beta_{2n} Z), \tag{4.16}$$

and the eigenvalues are given by

$$\beta_{1n}\tan(\beta_{2n}\tfrac{1}{2}\pi) = \beta_{2n}\tan(\beta_{1n}\tfrac{1}{2}\pi), \quad \beta_{1n} = \left(\beta_{2n}^2 + \frac{Re\,\sigma}{A^2}\right)^{\frac{1}{2}}. \tag{4.17}$$

Next, $\partial\hat{P}/\partial z$ at the liquid/gas interface is calculated in terms of ψ using the z-component of (3.7). The result is introduced in (4.6), which is solved for $\hat{f}$ subject to the conditions

$$\hat{f}(\pm\tfrac{1}{2}\pi) = 0, \quad \int_{-\pi/2}^{\pi/2} \hat{f}\,\mathrm{d}z = 0. \tag{4.18}$$

Finally, (4.5) and (4.7) are two homogeneous equations, and are arranged so that the solvability condition may be readily applied. The latter is obtained by taking the inner product of these equations with the adjoint eigenvectors, X_{en} and X_{en}^*. In the process, the biorthogonality condition is used, which states that

$$\int_{-\pi/2}^{\pi/2} (X_{en}, X_{en}^*) \begin{bmatrix} 0 & -1 \\ 1 & 2 \end{bmatrix} \begin{bmatrix} Z_{em} \\ Z_{em}^* \end{bmatrix} \mathrm{d}z = D_{nm}\,\delta_{nm}, \tag{4.19}$$

where δ_{nm} is the delta function ($\delta_{nm} = 0$, if $n \neq m$; $\delta_{nn} = 1$); D_{nm} is a constant, and (X_{en}, X_{en}^*) are the solutions to the adjoint eigenvalue problem:

$$\frac{\mathrm{d}^2}{\mathrm{d}z^2}\begin{bmatrix} X_{en} \\ X_{en}^* \end{bmatrix} = \begin{bmatrix} 0 & -\alpha_{1n}^2 \\ \alpha_{2n}^2 & -(\alpha_{1n}^2 + \alpha_{2n}^2) \end{bmatrix} \begin{bmatrix} X_{en} \\ X_{en}^* \end{bmatrix}, \tag{4.20}$$

$$X_{en}^* = \frac{\mathrm{d}X_{en}^*}{\mathrm{d}z} = 0, \quad z = \pm\tfrac{1}{2}\pi. \tag{4.21}$$

The form of the adjoint problem for the odd eigenfunctions is similar. The resulting homogeneous set of linear algebraic equations for each of the set of coefficients $\{C_{en}\}$ or $(C_{on}\}$ has a non-trivial solution when the determinant of the corresponding matrix is zero. Standard IMSL routines are used (DLFTCG, DLFDCG) for the calculation of this determinant.

The numerical procedure is the following:

(I) Given a set of parameters (A, Re), a value of σ is assumed according to results from the asymptotic theory ($Re \to \infty$), see Borkar & Tsamopoulos (1991) and Borkar (1989).

(II) The first N roots of (4.13) or (4.17) are generated using a Newton–Raphson scheme.

(III) These values of $\{\alpha_{1n}, \alpha_{2n}\}$ or $\{\beta_{1n}, \beta_{2n}\}$ are inserted into the solvability condition and the determinant of the matrix is calculated. If it is close to zero, the assumed value of σ is accepted upon verification with a larger value of N and the search is repeated for a new set of parameters; if it is not zero, this procedure is repeated with a new guess for σ.

This search is very tedious because, depending on the parameter values, up to $N = 60$ terms were required for convergence of the series and the calculated

determinant varied widely. Alternatively, the procedure suggested by Strani & Sabetta (1988) can be followed. Their physical problem is quite different from the one examined here and it is more readily amenable to semi-analytic calculations. However, here also the determinant of the homogeneous set of equations for the coefficients $\{C_{en}\}$ or $\{C_{on}\}$ can be solved for σ, which arises in these equations both explicitly and implicitly. Therefore, a Newton–Raphson procedure is needed and special care must be taken for a 'good' initial guess and for convergence to the specific eigenvalue sought. Truncation error of the infinite series may be significant and may introduce spurious wiggles even at the lower modes (see Strani & Sabetta 1988). Therefore, both these schemes are more reliable at high Re, where convergent values (with increasing N) were obtained and are used primarily in order to verify results from asymptotic theory and from numerical calculations which are presented next.

5. Numerical solution

Equations (3.6)–(3.14) will be reduced to an algebraic generalized eigenvalue problem for σ. To this end, they are discretized by the finite-element method. Velocity components, perturbed pressure, and perturbed shape are represented by biquadratic Lagrangian functions, $\phi_i(r,z)$, bilinear Lagrangian functions, $X_i(r,z)$, and quadratic Lagrangian functions $\Omega_j(z)$, respectively:

$$\left.\begin{aligned} \hat{u}(r,z) = \sum_{i=1}^{N} u_i \phi_i(r,z), \quad \hat{v}(r,z) = \sum_{i=1}^{N} v_i \phi_i(r,z), \quad \hat{w}(r,z) = \sum_{i=1}^{N} w_i \phi_i(r,z), \\ \hat{P}(r,z) = \sum_{i=1}^{M} P_i X_i(r,z), \quad \hat{f}(z) = \sum_{i=1}^{L} f_i \Omega_i(z), \end{aligned}\right\} \tag{5.1}$$

where L, M, and N are the number of coefficients in each expansion. Galerkin's procedure is employed in order to construct the residual equations. Equations (3.6), (3.7) and (3.12), are multiplied by the trial functions X_i, ϕ_i and Ω_i, respectively, and they are integrated over the domain. Integration by parts or the divergence theorem are applied, where necessary, in order to reduce second-order derivatives to first-order ones. Boundary conditions are directly applied on the boundary integrals. Thus, the weak form of the governing equation is obtained:

5.1. *Axisymmetric disturbances* ($k = 0, \hat{\boldsymbol{v}} = \hat{u}\boldsymbol{e}_r + \hat{w}\boldsymbol{e}_z$)

$$R_{ci} = \int_A X_i \nabla \cdot \hat{\boldsymbol{v}} \, \mathrm{d}A, \tag{5.2}$$

$$R_{Mi} = \int_A -\left[Re\,\sigma\hat{\boldsymbol{v}} + \frac{1}{r}(Re\,\hat{P} - \hat{\tau}_{\theta\theta})\,\boldsymbol{e}_r\right]\phi_i \,\mathrm{d}A + \int_A \nabla\phi_i \cdot (-Re\hat{P}\boldsymbol{I} + \hat{\boldsymbol{\tau}})\,\mathrm{d}A$$

$$+ \int_{-\pi/2}^{\pi/2} Re\,\phi_i\, 2\mathscr{H}_{\mathrm{p}} \boldsymbol{N}_{\mathrm{b}} f_{\mathrm{b}} \left[1 + \left(\frac{\partial f_{\mathrm{b}}}{\partial z}\right)^2\right]^{\frac{1}{2}} \mathrm{d}z, \tag{5.3}$$

$$R_{Ki} = \int_{-\pi/2}^{\pi/2} \Omega_i \left(-\sigma\hat{f} + \Lambda \frac{\partial f_{\mathrm{b}}}{\partial z}\hat{w} - \hat{u}\right)\mathrm{d}z. \tag{5.4}$$

The residuals, R_{ci}, R_{Mi} and R_{Ki} correspond to continuity, momentum and kinematic equations. In these general expressions $\mathrm{d}A = r\,\mathrm{d}r\,\mathrm{d}z$ with $0 \leqslant r \leqslant f_{\mathrm{b}}(z)$, $\frac{1}{2}\pi \leqslant z \leqslant \frac{1}{2}\pi$

and $2\mathscr{H}_p$ is given by (3.17). If $B = 0$, the base state reduces to a cylinder, $f_b = 1$ and $N_b = e_r$, and (5.3) and (5.4) are simplified. If $B \neq 0$, the base state must first be numerically calculated very accurately. To this end, (3.2)–(3.5) must be solved in a procedure similar to that employed by Tsamopoulos *et al.* (1988). Up to 100 quadratic elements have been used for this static problem. Numerical solutions compare very well to those obtained by Coriell *et al.* (1977) in terms of critical Bond numbers for different aspect ratios. Subsequently, f_b and its first and second derivatives are calculated, where required, using cubic splines. The second derivative $\partial^2\hat{f}/\partial z^2$ that arises in (3.17) must be further integrated by parts.

5.2. *Three-dimensional disturbances in zero gravity* ($B = 0, k \neq 0$)

In this case, the base state and the domain of integration are cylindrical, i.e. $f_b = 1$, $N_b = e_r\,(0 \leqslant r \leqslant 1, -\frac{1}{2}\pi \leqslant z \leqslant \frac{1}{2}\pi)$, and $2\mathscr{H}_p$ is given by (3.16). Galerkin's residual equations become

$$R_{ci} = \int_{-\pi/2}^{\pi/2}\int_0^1 X_i\left[\frac{1}{r}\frac{\partial}{\partial r}(r\hat{u}) - \frac{k}{r}\hat{v} + \Lambda\frac{\partial\hat{w}}{\partial z}\right] r\,dr\,dz, \tag{5.5}$$

$$\begin{aligned} R_{Mri} = \int_{-\pi/2}^{\pi/2}\int_0^1 \Bigg\{ & -Re\,\sigma\,\phi_i\hat{u} - Re\left(\frac{\partial\phi_i}{\partial r} + \frac{\phi_i}{r}\right)\hat{P} + 2\frac{\partial\phi_i}{\partial r}\frac{\partial\hat{u}}{\partial r} + 2\frac{\phi_i}{r^2}(\hat{u} - k\hat{v}) \\ & + \phi_i\frac{k}{r}\left[r\frac{\partial}{\partial r}\left(\frac{\hat{v}}{r}\right) + \frac{k}{r}\hat{u}\right] + \Lambda\frac{\partial\phi_i}{\partial z}\left(\frac{\partial\hat{w}}{\partial r} + \Lambda\frac{\partial\hat{u}}{\partial z}\right)\Bigg\} r\,dr\,dz \\ & + \int_{-\pi/2}^{\pi/2} Re\left[\Lambda^2\frac{\partial\phi_i}{\partial z}\frac{\partial\hat{f}}{\partial z} - \phi_i(1-k^2)\hat{f}\right] dz, \end{aligned} \tag{5.6}$$

$$\begin{aligned} R_{M\theta i} = \int_{-\pi/2}^{\pi/2}\int_0^1 \Bigg\{ & -Re\,\sigma\,\phi_i\hat{v} + Re\,\frac{\phi_i}{r}k\hat{P} + \left(\frac{1}{r}\frac{\partial\phi_i}{\partial r} - \frac{\phi_i}{r^2}\right)\left(r\frac{\partial\hat{v}}{\partial r} - \hat{v} + k\hat{u}\right) \\ & - 2\frac{k}{r^2}\phi_i(\hat{u} - k\hat{v}) + \Lambda\frac{\partial\phi_i}{\partial z}\left(\Lambda\frac{\partial\hat{v}}{\partial z} + k\frac{w}{r}\right)\Bigg\} r\,dr\,dz, \end{aligned} \tag{5.7}$$

$$\begin{aligned} R_{Mzi} = \int_{-\pi/2}^{\pi/2}\int_0^1 \Bigg\{ & -Re\,\sigma\,\phi_i\hat{w} - Re\frac{\partial\phi_i}{\partial z}\Lambda\hat{P} + \frac{\partial\phi_i}{\partial r}\left(\frac{\partial\hat{w}}{\partial r} + \Lambda\frac{\partial\hat{u}}{\partial z}\right) \\ & + \frac{k}{r}\phi_i\left(\Lambda\frac{\partial\hat{v}}{\partial z} + \frac{k}{r}\hat{w}\right) + 2\Lambda^2\frac{\partial\phi_i}{\partial z}\frac{\partial\hat{w}}{\partial z}\Bigg\} r\,dr\,dz, \end{aligned} \tag{5.8}$$

$$R_{Ki} = \int_{-\pi/2}^{\pi/2} \Omega_i(\sigma\hat{f} + \hat{u})\,dz. \tag{5.9}$$

The residuals $R_{Mri}, R_{M\theta i}, R_{Mzi}$ correspond to the three components of the momentum equation.

Equations (5.2)–(5.4) or (5.5)–(5.9) constitute a generalized eigenvalue problem of the form

$$\boldsymbol{A}\boldsymbol{x} = \sigma\boldsymbol{B}\boldsymbol{x}, \tag{5.10}$$

where $\boldsymbol{A}$ and $\boldsymbol{B}$ are coefficient matrices and $\boldsymbol{x}$ is the eigenvector corresponding to the eigenvalue σ. An IMSL routine (DGVLRG) is used first in order to calculate the complex eigenvalues for a set of parameters. Owing to the large memory and storage requirements the eigenvectors cannot be calculated directly using any commercial

software. Instead, for a given value of σ, (5.10) is rearranged into an algebraic set of equations for $\boldsymbol{x}$:

$$(\boldsymbol{A}-\sigma\boldsymbol{B})\,\boldsymbol{x}=\boldsymbol{0}. \tag{5.11}$$

A non-trivial solution to (5.11) is obtained by setting $\hat{P}(r=0, z=\frac{1}{2}\pi)=1.0$ which makes the matrix $(\boldsymbol{A}-\sigma\boldsymbol{B})$ non-singular. This complex matrix has an arrow structure and is inverted by the efficient routine developed by Thomas & Brown (1987). The real parts of the complex eigenvectors correspond to the physical variables of the problem.

Several tests for accuracy of the numerical results have been performed:

(I) For $B=k=0$ and $Re \geqslant 1000$, numerically computed eigenvalues agree very well with those obtained from the boundary-layer analysis (Borkar & Tsamopoulos 1991).

(II) For $B=k=0$, $Re=100$, 1000 and $\Lambda=2$, numerically computed eigenvalues agree very well with those obtained from the analytical method presented in §4. Furthermore, Borkar (1989) has solved (4.2)–(4.6) by separation of variables after substituting the no-slip condition with the shear-free condition on the two solid/liquid interfaces. This modification allows for a much simpler analysis than that presented in §4 and still gives quite accurate results. These results compare well with the numerically computed ones.

(III) The numerical algorithms for non-axisymmetric or non-zero gravity calculations reproduce exactly the results obtained earlier for $B=k=0$.

(IV) Convergence of eigenvalues has been verified by refinement of the mesh in both the r- and z-directions, see table 1. Eight elements were found to be sufficient in the radial direction. However, more elements are required in the axial direction in order to achieve at least 3 digits of accuracy in the first mode, especially for $Re=1000$ or larger. Unfortunately, the number of elements is restricted by either the virtual memory of the IBM 3090 at CNSF or the maximum size of matrix allowed by the software employed (IMSL or ESSL). It was found that the number of elements can be as high as eight radial and twelve axial.

Such a discretization generates the matrices $\boldsymbol{A}$ and $\boldsymbol{B}$ each of size (899×899). Then, solution of the eigenvalue problem (5.10) requires 5600 s of CPU on an IBM 3084 at the University of Buffalo or 650 s of CPU on the IBM 3090 at CNSF. Calculation of each eigenvector (5.11) requires only 70 s of CPU on an IBM 3084. It was also found that as B and/or $1/\Lambda$ increase towards the stability limit, the accuracy decreases. For example, if $B=2.5, \Lambda=2.0$, the first eigenvalue is correct to only one digit irrespective of the accuracy achieved in calculating the corresponding static shape. As a result, eigenvalues will be reported here only to the computed accuracy.

On the other hand, if $B=0$ and for any integer value of k, the computational effort and requirements may be reduced by a factor of two or the accuracy may be increased. This is achieved by calculating separately the symmetric and anti-symmetric modes of the system. In the process, proper boundary conditions must be set at $z=0$, so that only half of the domain is discretized $(0 \leqslant r \leqslant 1, 0 \leqslant z \leqslant \frac{1}{2}\pi)$. These conditions are

5.3. *Symmetric modes*

Shapes of liquid bridges are symmetric about the midplane when

$$\partial \hat{f}/\partial z=0, \quad z=0. \tag{5.12}$$

Mesh size ($r \times z$)	$n = 1$		$n = 2$		$n = 3$		$n = 4$	
	σ_r	σ_i	σ_r	σ_i	σ_r	σ_i	σ_r	σ_i
5×5	0.01471	5.0894	0.0502	11.3859	0.109	20.216	0.232	36.28
8×8	0.01505	5.0813	0.0501	11.2002	0.1077	19.005	0.187	28.34
7×14*	0.01567	5.0821	0.0485	11.1699	0.1031	18.787	0.178	27.49
8×14*	0.01557	5.0821	0.0483	11.1683	0.1022	18.780	0.179	27.47
8×16*	0.01572	5.0828	0.0480	11.1679	0.1027	18.770	0.176	27.42

TABLE 1. Eigenvalues of the first four axisymmetric modes with varying mesh size and for $Re = 1000$, $A = 2$. Reported mesh sizes are equivalents for the full domain. An asterisk indicates that computation was carried out in a half-domain.

Solutions then correspond to the odd modes in §4, so that shapes are described by a summation of cosines. Moreover, the radial and azimuthal components of velocity must be symmetric and the axial component of velocity must be zero.

$$\partial\hat{u}/\partial z = \partial\hat{v}/\partial z = \hat{w} = 0, \quad z = 0. \tag{5.13}$$

By using (3.6) and (5.13) it may also be shown that

$$\partial\hat{w}/\partial z = \text{const}, \quad z = 0. \tag{5.14}$$

Finally, introducing (5.13) and (5.14) in the axial component of the momentum equation results in

$$\partial\hat{P}/\partial z = 0, \quad z = 0. \tag{5.15}$$

5.4. *Antisymmetric modes*

Antisymmetric shapes of liquid bridges arise when the radial and azimuthal components of velocity assume the same numerical value, but opposite signs above and below the midplane:

$$\hat{u}|_{z=+\Delta z} = -\hat{u}|_{z=-\Delta z}, \qquad \hat{v}|_{z=+\Delta z} = -\hat{v}|_{z=-\Delta z}. \tag{5.16}$$

Since velocity is a continuous function, it follows that

$$\hat{u} = \frac{\partial^n \hat{u}}{\partial r^n} = \hat{v} = \frac{\partial^n \hat{v}}{\partial r^n} = 0, \quad z = 0, \quad n = 1, 2, \ldots. \tag{5.17}$$

Combining (5.17) and (3.6) yields

$$\frac{\partial \hat{w}}{\partial z} = 0, \quad z = 0. \tag{5.18}$$

Also, due to (5.16) and (5.17),

$$\left.\frac{\partial \hat{u}}{\partial z}\right|_{z=+\Delta z} = \left.\frac{\partial \hat{u}}{\partial z}\right|_{z=-\Delta z}, \tag{5.19}$$

and in the limit of $\Delta z \to 0$,

$$\frac{\partial^2 \hat{u}}{\partial z^2} = 0, \quad z = 0. \tag{5.20}$$

Substitution of (5.17), (5.18) and (5.20) into the radial component of the momentum equation reduces it to $\partial\hat{P}/\partial r\,(z=0)=0$, which upon integration gives

$$\hat{P} = \text{const}, \quad z = 0. \tag{5.21}$$

Without loss of generality, this constant is taken to be equal to zero. Finally, according to the kinematic condition,

$$\hat{f} = 0, \quad z = 0. \tag{5.22}$$

Numerical solutions of antisymmetric modes correspond to the even modes of §4, where shapes are described by summation of sines.

Eigenvalues and eigenvectors computed using the above-derived boundary conditions with eight radial and four axial elements in the half-domain are in excellent agreement with those computed with eight radial and eight axial elements in the full domain. Finer discretization was performed in the axial direction until four significant digits were accurately calculated for the primary eigenvalue. This required eight axial elements. The size of each matrix with this (8×8) finite-element mesh in the half-domain reduces to (599×599). Solution of the eigenvalue problem (5.10) requires 1400 s of CPU on an IBM 3084.

When the Rayleigh limit is approached ($\Lambda = 0.5$) the primary eigenvalue gets very close to zero (bifurcation point). Then, 12 axial elements were used for the half-domain in order to get accurate results. When the Rayleigh limit is exceeded ($\Lambda = 0.45$) the first eigenvalue becomes negative (unstable system), but this refined mesh is still more than adequate.

6. Results and discussion

According to the normal-mode analysis, (3.18), the liquid bridge undergoes a linearly stable motion if $\sigma_r > 0$, or it is linearly unstable if $\sigma_r < 0$. The stable motion is either an underdamped oscillation if $\sigma_i \neq 0$ or an overdamped oscillation if $\sigma_i = 0$. The effect of the various parameters of the system on the eigenvalues and eigenvectors is discussed next. The reported results are based on the finite-element calculations and coincide with the analytical ones when the latter converge.

6.1. *Axisymmetric disturbances in zero gravity* ($k = B = 0$)

In the absence of gravity, a static liquid bridge of volume $\tilde{V} = \pi\tilde{R}^2\tilde{L}$ has a cylindrical stable shape if the ratio $\tilde{L}/\tilde{R}$ is below the Rayleigh limit of 2π. This requirement translates into $\Lambda > 0.5$ according to the present definition of aspect ratio ($\Lambda = \pi\tilde{R}/\tilde{L}$). When $B = k = 0$, the particular response of the liquid bridge to infinitesimal and axisymmetric disturbances depends only on the modified Re and on Λ. If $\tilde{R} = 0.5$ cm, $Re \approx 550$ for uncontaminated water, whereas it is expected to vary between 2 and 50 for most molten semiconductors and ceramics, depending on the temperature.

Figures 2 and 3 show the damping rate (σ_r) and frequency (σ_i) of the first four modes as a function of the aspect ratio and for $Re = 10$ and 500, respectively. The very good agreement between the present results for σ_i at $Re = 500$ and the inviscid theory (Sanz 1985) should be noted. Clearly, the inviscid theory would predict $\sigma_r = 0$ for all parameter values. As expected, the higher modes exhibit larger σ_r and σ_i for the same values of Λ and Re. Furthermore, increasing Λ results in larger damping rates of each mode even when Re is larger. This is due to the more significant viscous dissipation that occurs in the increased solid/liquid contact area for the same zone

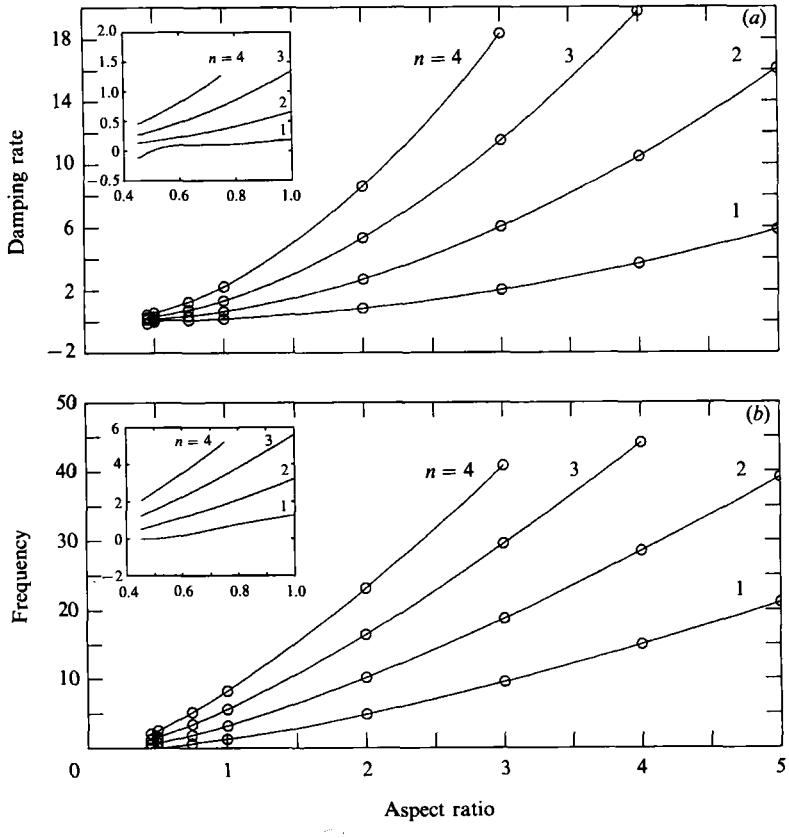

FIGURE 2. (*a*) Damping rate and (*b*) frequency of the first four axisymmetric modes as a function of aspect ratio for $Re = 10$. Open circles indicate numerical results of this work.

length. Similarly, increasing Λ results in larger frequencies due to the relatively decreased side area and the more restrained motion of fluid. Tables 2 and 3 provide the eigenvalues for the first four modes. The real part of the first eigenvalue is very nearly zero at $\Lambda = 0.5$ and becomes negative at $\Lambda = 0.45$ for either value of Re. Consequently, the first mode becomes unstable at $\Lambda = 0.5$, whereas the higher ones remain stable in accordance with results from static analysis.

The effect of the modified Re on the system eigenvalues is shown in figure 4 for $\Lambda = 2$. Increasing Re results in reduced values for the damping rates to almost zero values for all modes. At the same time the existence of multiple eigenvalues with real parts close to zero for $Re > 500$ makes computations harder. The inviscid theory (Sanz 1985) predicts zero damping irrespective of Re, whereas the boundary-layer theory (Borkar & Tsamopoulos 1991) becomes asymptotically correct for $Re > 50$ and more so for the lower mode. Increasing Re results in increased values for the frequency, which asymptotically approach the predictions of the boundary-layer theory for every mode considered. As Re decreases below approximately 3, the frequencies drop sharply towards zero. Unfortunately, our calculations had limited accuracy and identifying each computed eigenmode became a very difficult task for $Re < 2.5$. However, it is anticipated that there will be values of Re at which the oscillations will become overdamped, i.e. the two complex conjugate eigenvalues will be replaced by two real and positive ones (see Prosperetti 1980 and Strani & Sabetta 1988). As seen in figure 4 (*b*), this occurs for the higher modes first ($n = 4$), and as Re

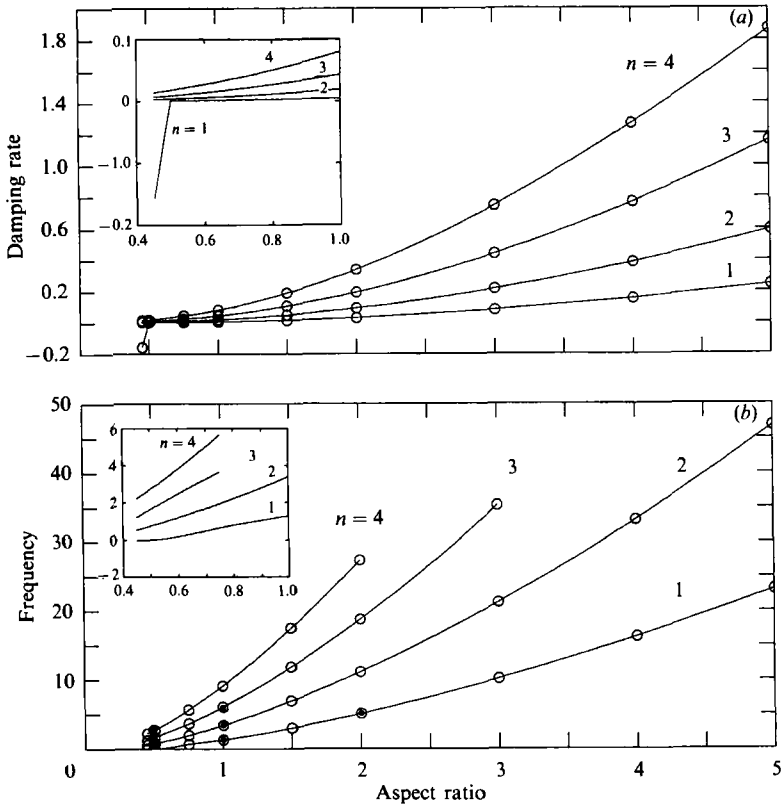

FIGURE 3. (*a*) Damping rate and (*b*) frequency of the first four axisymmetric modes as a function of aspect ratio for $Re = 500$. Open circles indicate numerical results of this work, solid circles indicate results by Sanz & Diez (1989). In the insert and for $0.45 \leqslant \Lambda \leqslant 0.5$ straight lines have been used to connect numerical results.

	$n = 1$		$n = 2$		$n = 3$		$n = 4$	
Λ	σ_r	σ_i	σ_r	σ_i	σ_r	σ_i	σ_r	σ_i
5	5.824	21.09	16.08	39.12	29.97	59.88	47.03	81.18
4	3.698	15.01	10.49	28.51	19.75	44.16	31.17	60.30
3	2.032	9.554	6.016	18.77	11.51	29.55	18.32	40.83
2	0.846	4.859	2.706	10.19	5.31	16.43	8.61	23.14
1	0.187	1.273	0.656	3.22	1.35	5.61	2.26	8.25
0.75	0.104	0.638	0.362	1.86	0.75	3.42	1.28	5.19
0.5	10^{-13}	0	0.162	0.72	0.33	1.56	0.56	2.54
0.45	−0.123	0.000	0.133	0.51	0.26	1.23	0.45	2.07
	0.203	0.000	—	—	—	—	—	—

TABLE 2. Real and imaginary part of eigenvalues of the first four axisymmetric modes with varying aspect ratio and for $Re = 10$

decreases further the lower modes seem to follow the same pattern. Table 4 provides the calculated eigenvalues.

Typical shapes for the first four modes are shown in figure 5. They comprise part of the calculated eigenvectors. According to the analysis in §4, shapes of

	$n=1$		$n=2$		$n=3$		$n=4$	
A	σ_r	σ_i	σ_r	σ_i	σ_r	σ_i	σ_r	σ_i
5	0.244	23.13	0.595	46.80	1.16	77.31	1.87	111.5
4	0.152	16.25	0.384	33.19	0.77	54.94	1.27	79.45
3	0.079	10.18	0.214	21.23	0.44	35.28	0.75	51.18
2	0.029	5.08	0.091	11.16	0.19	18.75	0.34	27.39
1.50	0.014	2.99	0.048	6.95	0.10	11.86	0.19	17.48
1	0.0048	1.30	0.019	3.40	0.043	6.07	0.08	9.14
0.75	0.0025	0.65	0.010	1.94	0.023	3.65	0.043	5.65
0.5	0.0009	0.002	0.004	0.74	0.009	1.63	0.018	2.71
0.45	−0.157	0.00	0.003	0.53	0.007	1.20	0.014	2.20

TABLE 3. Real and imaginary part of eigenvalues of the first four axisymmetric modes with varying aspect ratio and for $Re = 500$

antisymmetric modes can be expressed in terms of an infinite summation of sines and shapes of symmetric ones in terms of summation of cosines. Alternatively, the calculated shapes may be decomposed into Fourier series. The Fourier coefficients are calculated in the usual way:

$$a_m = \frac{2}{\pi}\int_{-\pi/2}^{\pi/2} \hat{f}(z)\cos(2mz)\,\mathrm{d}z, \quad m = 0, 1, 2, \ldots, \tag{6.1}$$

$$b_m = \frac{2}{\pi}\int_{-\pi/2}^{\pi/2} \hat{f}(z)\sin(2mz)\,\mathrm{d}z, \quad m = 1, 2, 3, \ldots. \tag{6.2}$$

Table 5 gives the Fourier coefficients of the first ($n = 1$) axisymmetric mode for $Re = 10, 500$. Note that all the coefficients of the cosine series are practically zero. In particular, $a_0 = 10^{-9}$; this small value of the zeroth coefficient reaffirms the high accuracy with which the volume of the liquid bridge is conserved. Moreover, b_1 is more dominant and coefficients decrease faster for $Re = 500$ than for $Re = 10$. Consequently, more Fourier modes and correspondingly more terms in the infinite summation in §4 are required for a converged solution as Re decreases. Similarly, all the coefficients of the sine series are practically zero, when the second or any symmetric shape with respect to the $z = 0$ plane is decomposed.

6.2. *Axisymmetric disturbances with gravity* ($k = 0, B \neq 0$)

In experiments that have taken place in spacecraft, gravity is reduced to as low as 10^{-4} g and may become time-dependent owing to orbital motion (Zhang & Alexander 1990). On the other hand, in earthbound applications gravity is always present and deforms the static cylindrical shape to an 'amphora-like' shape. In these experiments, and for liquid bridges with $\tilde{R} = \tilde{L} = 0.5$ cm, the Bond number for uncontaminated water is 1.1 and for most liquids of interest ($\gamma \approx 30$ g/s^2) it is 2.6. Coriell *et al.* (1977) used variational calculus to determine stability of static shapes under gravity. They found that the critical B beyond which the bridge became unstable depended on the aspect ratio (see their figure 6).

In a more general setting, Tsamopoulos *et al.* (1988) showed that the Rayleigh limit is a subcritical bifurcation from stable cylindrical shapes to unstable sinusoidal ones in an amplitude *vs.* aspect ratio plot; see the bifurcation point at $\alpha = 0.15915$ in their figure 2, which corresponds to the first bifurcation point for instability of a

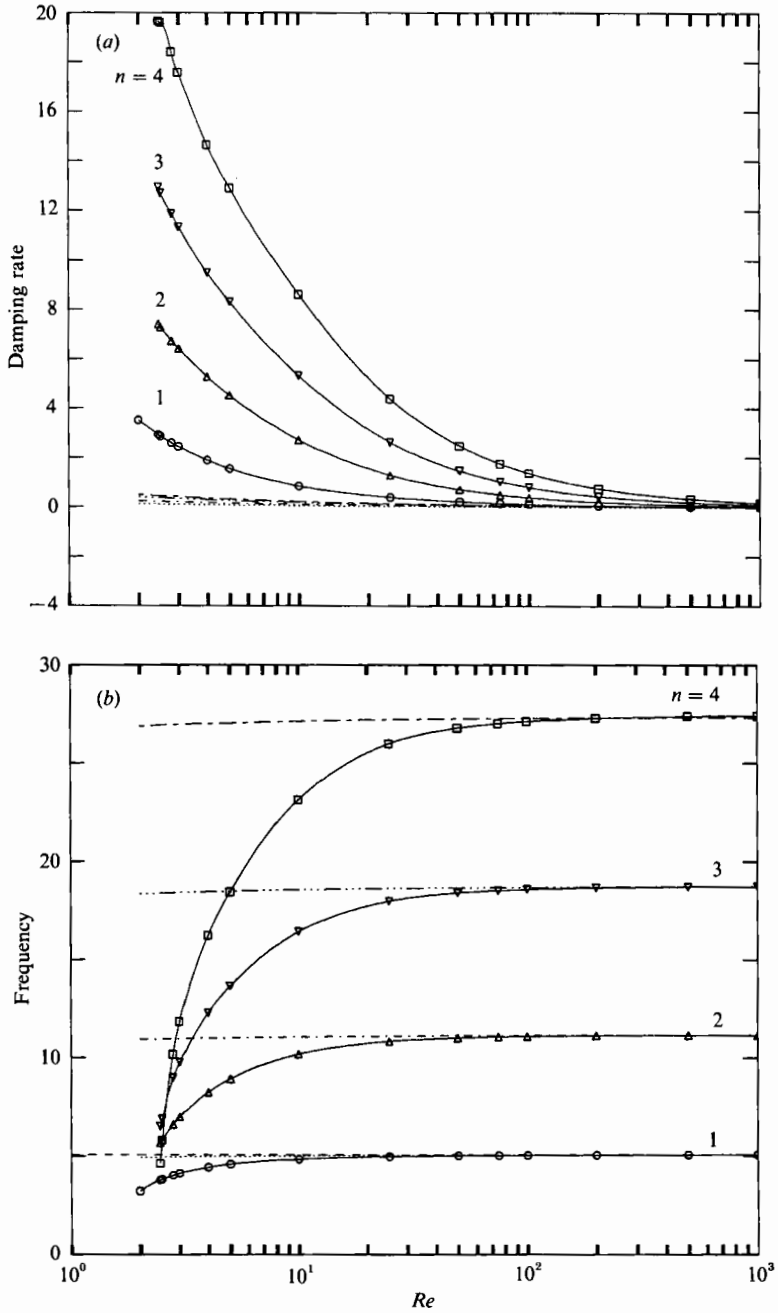

FIGURE 4. (*a*) Damping rate and (*b*) frequency of $n = 1$ (○, ...), $n = 2$ (△, –·–), $n = 3$ (▽, –···–) and $n = 4$ (□, ————) as a function of Reynolds number for $\Lambda = 2$. Continuous lines connect numerical values from this work, discontinuous lines are from the boundary-layer analysis by Borkar & Tsamopoulos (1991). The dashed line in (*b*) is the inviscid result by Sanz & Diez (1989).

cylindrical column. When gravity is present, this bifurcation is broken, and the originally stable family of cylindrical shapes exhibits a limit point, the location of which depends on B (see domain $0.14 < \alpha < 0.2$ in their figures 13 and 14).

	$n = 1$		$n = 2$		$n = 3$		$n = 4$	
Re	σ_r	σ_i	σ_r	σ_i	σ_r	σ_i	σ_r	σ_i
1000	0.016	5.083	0.048	11.17	0.101	18.77	0.176	27.42
500	0.029	5.080	0.091	11.16	0.192	18.75	0.337	27.39
200	0.065	5.073	0.208	11.14	0.434	18.70	0.754	27.28
100	0.119	5.060	0.385	11.10	0.799	18.61	1.368	27.12
75	0.152	5.052	0.496	11.07	1.027	18.55	1.751	27.01
50	0.215	5.036	0.708	11.02	1.458	18.43	2.470	26.78
25	0.388	4.991	1.283	10.84	2.614	18.00	4.374	25.98
10	0.846	4.859	2.706	10.19	5.313	16.43	8.607	23.14
5	1.549	4.601	4.517	8.922	8.301	13.65	12.90	18.47
4	1.885	4.442	5.269	8.240	9.484	12.28	14.65	16.25
3	2.432	4.126	6.413	7.007	11.35	9.76	17.57	11.84
2.8	2.587	4.021	6.729	6.617	11.87	8.98	18.40	10.17
2.5	2.86	3.81	7.29	5.83	12.7	6.9	19.6	5.8
2.45	2.92	3.77	7.41	5.67	12.9	6.5	19.7	4.6

TABLE 4. Real and imaginary part of eigenvalues of the first four axisymmetric modes with varying Reynolds number and for $\Lambda = 2$

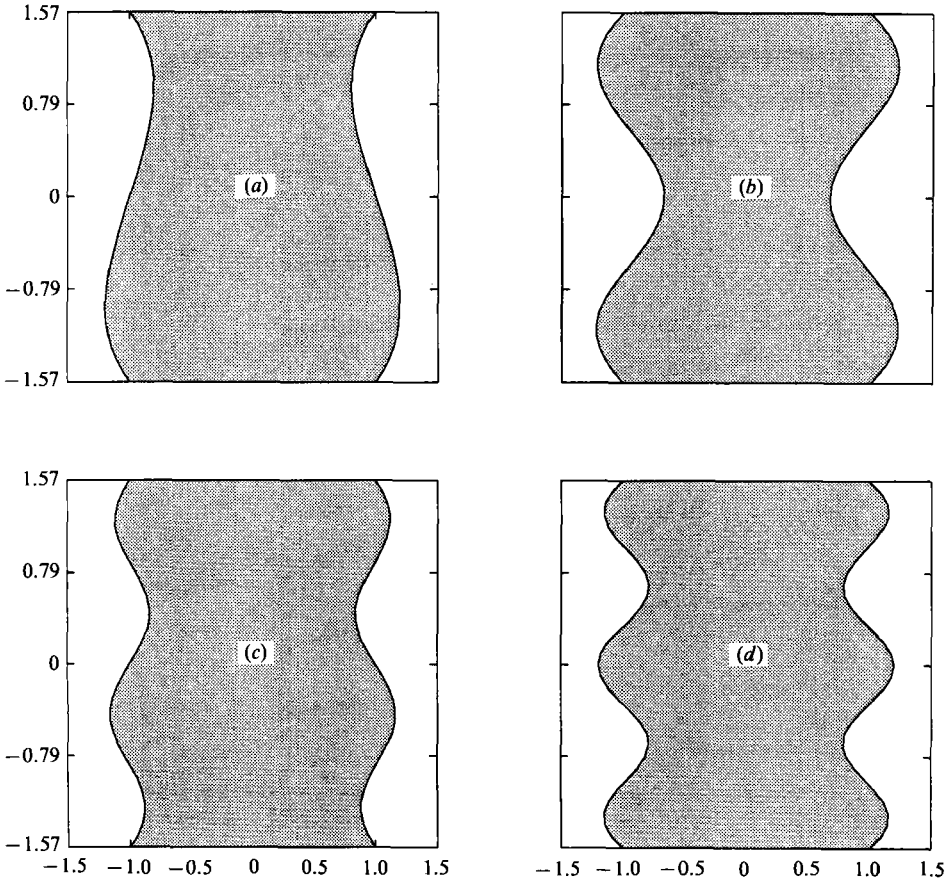

FIGURE 5. Typical shapes of floating zone without gravitational effects for (*a*) first, (*b*) second, (*c*) third and (*d*) fourth mode under an axisymmetric disturbance, with $Re = 10$, $\Lambda = 2$.

	$Re = 10$		$Re = 500$	
m	a_m ($\times 10^8$)	b_m ($\times 10^3$)	a_m ($\times 10^8$)	b_m ($\times 10^4$)
0	0.04	—	0.16	—
1	0.69	−38.9	−2.4	1360.0
2	−0.39	5.88	0.71	−91.7
3	0.35	−1.79	−0.85	26.6
4	−0.12	0.799	0.17	−11.1
5	−0.22	−0.445	0.96	5.71
6	−0.27	0.278	0.85	−3.43
7	0.12	−0.188	−0.24	2.14
8	−0.07	0.125	0.07	−1.37
9	0.26	−0.0954	−0.76	0.778
10	0.33	0.0628	1.3	−0.736
11	0.11	−0.0442	0.10	0.597
12	−0.09	0.0492	0.83	−0.370
13	−0.71	−0.0224	2.4	0.0917
14	−0.06	0.0197	0.044	−0.0693

TABLE 5. Fourier coefficients predicted by decomposing the interface shape of the first axisymmetric mode with $Re = 10$ and 500 and for $\Lambda = 2$, $B = 0$

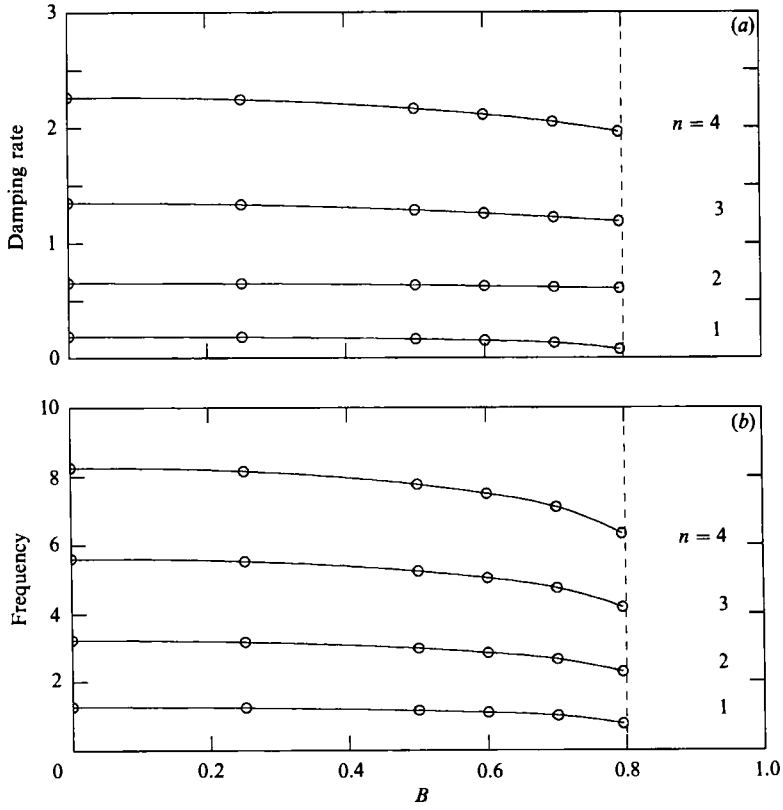

FIGURE 6. (*a*) Damping rate and (*b*) frequency of the first four axisymmetric modes as a function of Bond number for $Re = 10$, $\Lambda = 1$. Open circles indicate numerical results of this work. The vertical dashed line indicates location of limit point in static analysis.

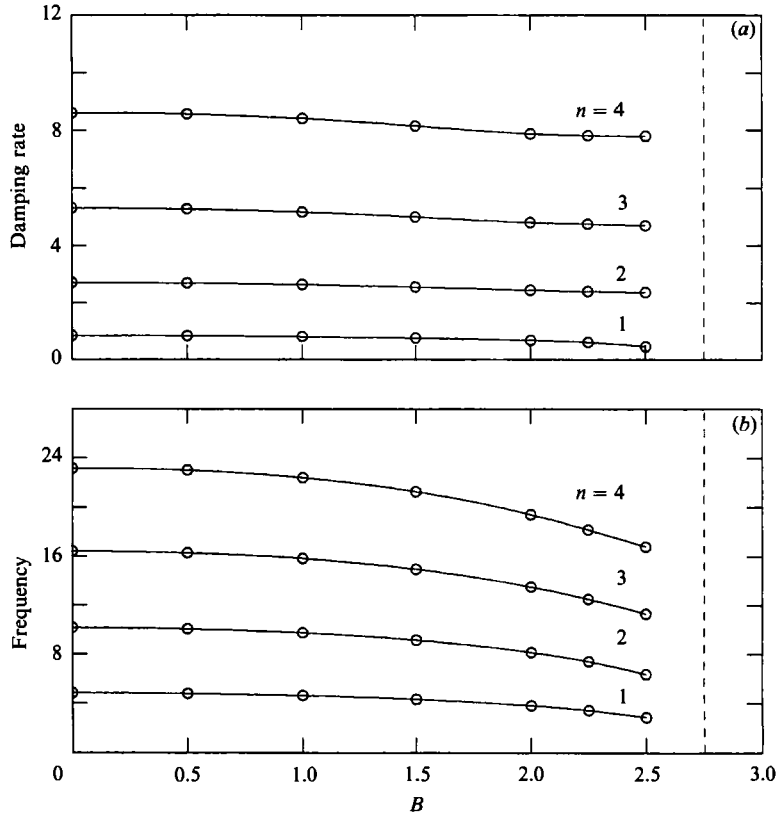

FIGURE 7. As figure 6, but for $\Lambda = 2$.

Consequently, the analysis of Coriell *et al.* was confirmed and related to that of Rayleigh. Beyond the limiting values of aspect ratio, static solutions either do not exist or they appear in pairs both of which are unstable. In the present study, axisymmetric eigensolutions will be computed only for combinations of Λ and B for which static shapes exist and are stable.

The damping rate and oscillation frequency as a function of B are shown in figures 6 and 7 for $\Lambda = 1$ and 2 respectively. The limiting Bond number in the former case is approximately 0.8 and in the latter it is 2.75. The modified Reynolds number is 10 in both cases.

The accuracy of the computed values decreases as B approaches the stability limit. Keeping all other parameters the same, eigenvalues increase as Λ increases. It is also observed that for all modes and aspect ratios examined both damping rate and frequency decrease as B increases. This is because static shapes under gravity resemble the eigenfunctions more than the cylindrical shapes do (see figure 8). Therefore, less energy is required for (i.e. lower frequency) and consumed by (i.e. lower damping rate) the underdamped oscillations. At the stability limit itself the real part of the first eigenvalue will change sign and this mode and the liquid bridge will become unstable. Tables 6 and 7 give the calculated eigenvalues for $\Lambda = 1$ and 2, respectively.

Figure 9 shows the variation of the eigenvalues with Re for $B = 1$ and $\Lambda = 2$. Effects similar to those discussed for $B = 0$ are observed here also. For example, the

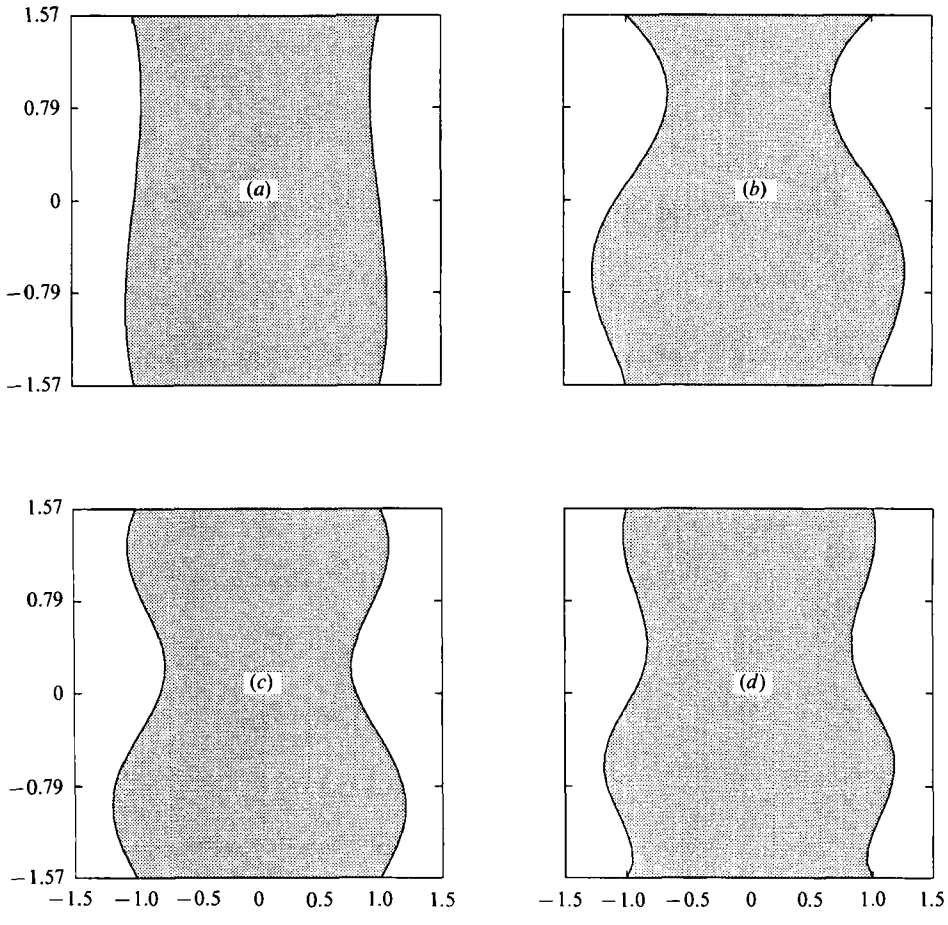

FIGURE 8. Typical shapes of floating zone with gravitational effects for (*a*) unperturbed state, (*b*) first mode, (*c*) second mode and (*d*) third mode, under an axisymmetric disturbance with $B = 1$, $Re = 10$, $\Lambda = 2$.

	$n = 1$		$n = 2$		$n = 3$		$n = 4$	
B	σ_r	σ_i	σ_r	σ_i	σ_r	σ_i	σ_r	σ_i
0.25	0.181	1.249	0.651	3.167	1.33	5.53	2.24	8.15
0.50	0.164	1.166	0.636	2.975	1.28	5.24	2.16	7.77
0.60	0.151	1.104	0.627	2.841	1.25	5.04	2.11	7.50
0.70	0.130	1.009	0.617	2.649	1.22	4.75	2.04	7.11
0.795	0.07	0.77	0.60	2.28	1.1	4.1	1.9	6.3

TABLE 6. Real and imaginary part of eigenvalues of the first four axisymmetric modes with varying Bond number for $Re = 10$, $\Lambda = 1$

damping rate asymptotically approaches zero as Re increases, higher modes exhibit higher damping rates and frequencies, and as Re decreases the motion becomes overdamped. As explained in §5, calculations with gravity are more costly since a plane of symmetry or antisymmetry ($z = 0$) no longer exists. Consequently,

	$n = 1$		$n = 2$		$n = 3$		$n = 4$	
B	σ_r	σ_i	σ_r	σ_i	σ_r	σ_i	σ_r	σ_i
0.5	0.837	4.808	2.688	10.08	5.28	16.30	8.57	23.00
1.0	0.810	4.647	2.635	9.76	5.17	15.83	8.41	22.38
1.5	0.762	4.345	2.548	9.17	5.00	14.95	8.15	21.25
2.0	0.683	3.828	2.444	8.16	4.81	13.51	7.88	19.41
2.25	0.613	3.437	2.399	7.41	4.76	12.50	7.82	18.2
2.5	0.46	2.86	2.37	6.36	4.7	11.3	7.8	16.8

TABLE 7. Real and imaginary part of eigenvalues of the first four axisymmetric modes with varying Bond number for $Re = 10$, $\Lambda = 2$

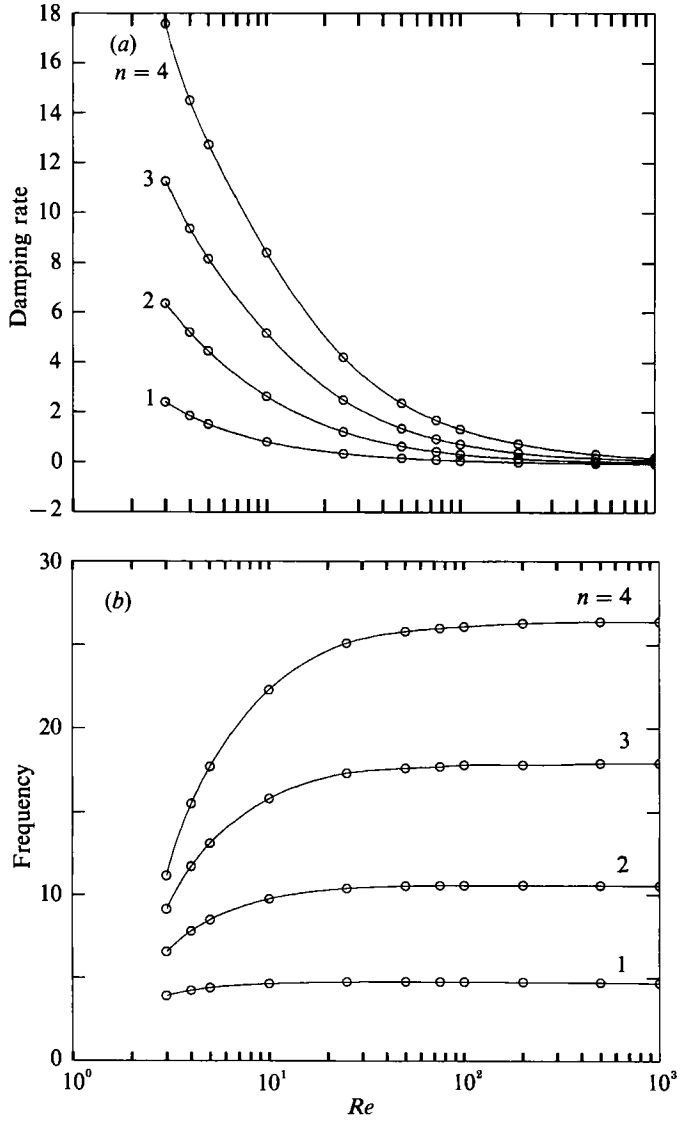

FIGURE 9. (*a*) Damping rate and (*b*) frequency of the first four axisymmetric modes as a function of Reynolds number for $\Lambda = 2$, $B = 1$. Open circles indicate numerical results of this work.

	$n = 1$		$n = 2$		$n = 3$		$n = 4$	
Re	σ_r	σ_i	σ_r	σ_i	σ_r	σ_i	σ_r	σ_i
1000	−0.054	4.69	0.008	10.5	0.08	17.9	0.17	26.4
500	−0.042	4.73	0.034	10.5	0.16	17.9	0.32	26.4
200	0.001	4.76	0.138	10.5	0.37	17.8	0.74	26.3
100	0.059	4.77	0.312	10.5	0.72	17.8	1.32	26.1
75	0.093	4.77	0.423	10.5	0.93	17.7	1.68	26.0
50	0.159	4.77	0.634	10.5	1.35	17.6	2.36	25.8
25	0.339	4.76	1.21	10.4	2.49	17.3	4.21	25.1
10	0.810	4.65	2.64	9.76	5.17	15.8	8.41	22.3
5	1.519	4.395	4.45	8.52	8.17	13.1	12.7	17.7
4	1.856	4.235	5.21	7.84	9.36	11.7	14.5	15.5
3	2.404	3.910	6.37	6.59	11.26	9.1	17.5	11.1

TABLE 8. Real and imaginary part of eigenvalues of the first four axisymmetric modes with varying Reynolds number for $B = 1$, $\Lambda = 2$

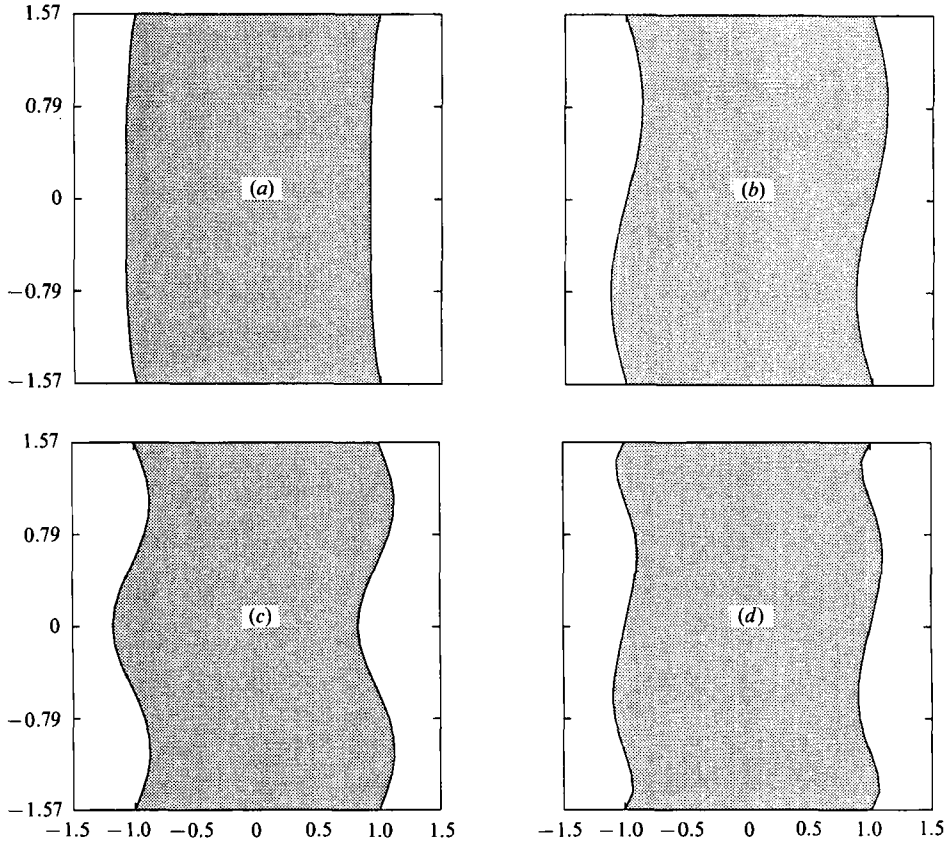

FIGURE 10. Typical shapes of floating zone without gravitational effect for (*a*) zeroth, (*b*) first, (*c*) second and (*d*) third mode, under a non-axisymmetric disturbance, with $Re = 10$, $\Lambda = 2$, $k = 1$.

calculations with values of Re below 3 were not pursued. Numerical results are shown in table 8. This table reveals more clearly that even though the static bridge is stable (since $B = 1, \Lambda = 2$), when perturbed and Re is large it may become unstable.

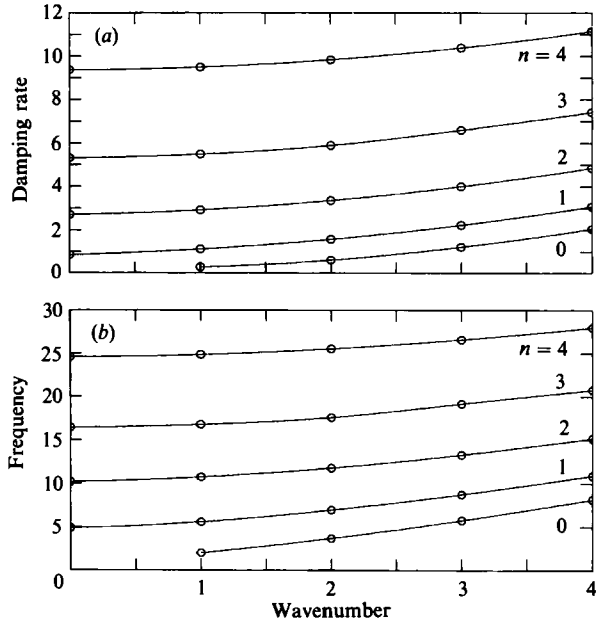

FIGURE 11. (*a*) Damping rate and (*b*) frequency of the first five non-axisymmetric modes as a function of wavenumber for $Re = 10$, $A = 2$. Open circles indicate numerical results of this work.

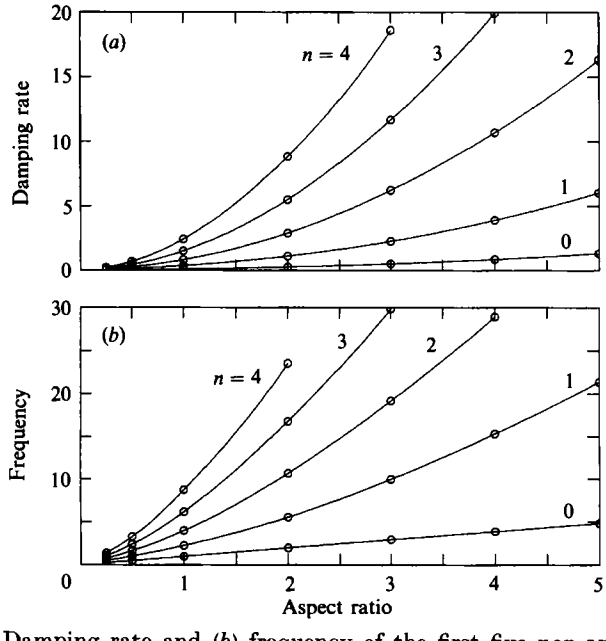

FIGURE 12. (*a*) Damping rate and (*b*) frequency of the first five non-axisymmetric modes as a function of aspect ratio for $Re = 10$, $k = 1$. Open circles indicate numerical results of this work.

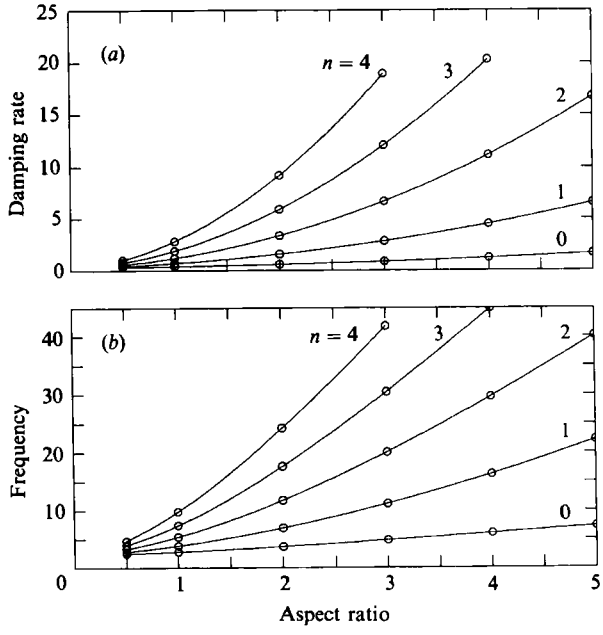

FIGURE 13. As figure 12 but for $k = 2$.

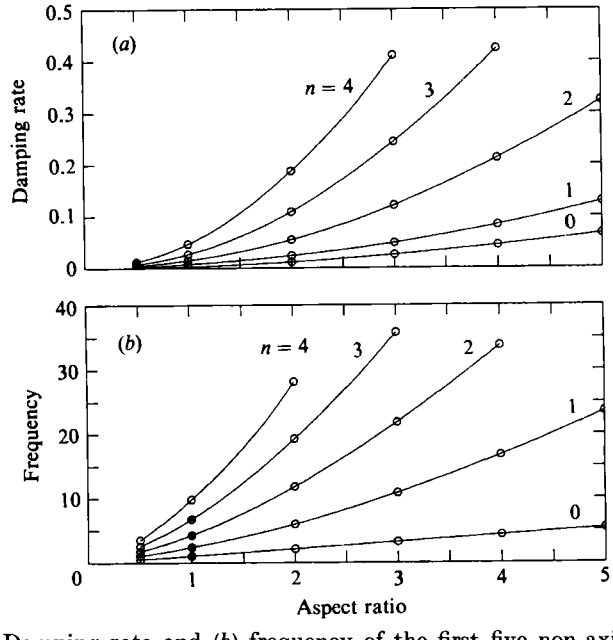

FIGURE 14. (*a*) Damping rate and (*b*) frequency of the first five non-axisymmetric modes as a function of aspect ratio for $Re = 1000$, $k = 1$. Open circles indicate numerical results of this work, solid circles indicate results by Sanz & Diez (1989).

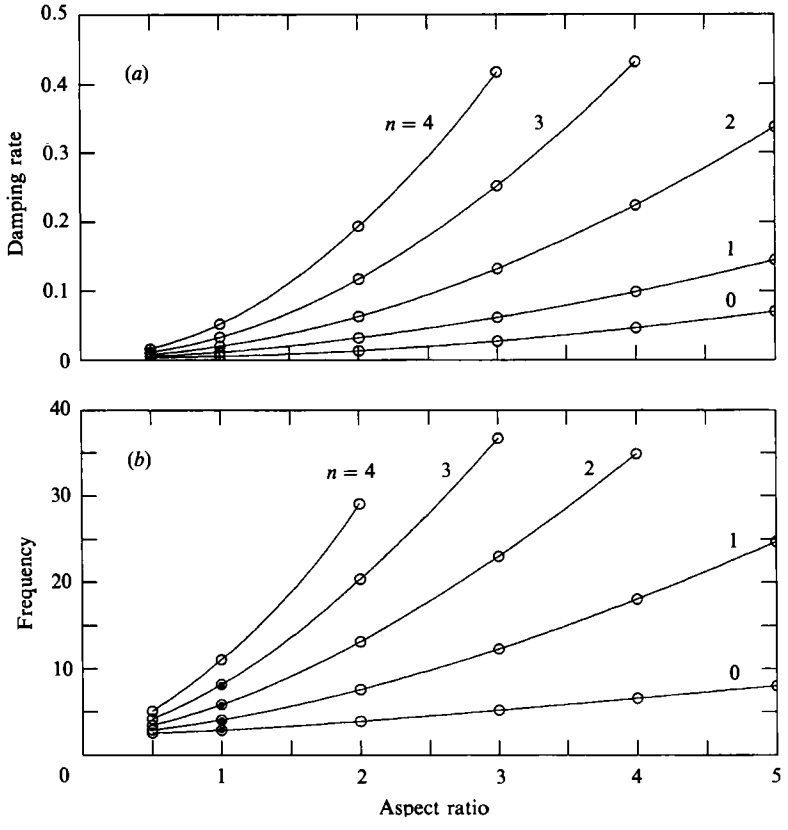

FIGURE 15. As figure 14 but for $k = 2$.

As explained in the Introduction, the surface tension of the material can be measured first by a static method. In addition, forced or free oscillations may be used for its dynamic measurement. However, the eigenfrequency exhibits a weak dependence on Re for Re as low as 5, when $n = 1$ (the easier mode to excite), whereas the damping rate exhibits a strong enough dependence on Re, for $Re < 50$, see figures 4 and 9. It should be noted here that most molten ceramics and semiconductors are expected to fall in this range. Therefore, for reliable measurements of both surface tension and viscosity using only dynamic data from this work, it is necessary to first measure frequency and damping rate for perhaps one (or two) values of A, then assume a value for γ which sets the timescale in order to calculate the dimensionless frequency and damping rate, and finally use these in the appropriate figures to deduce values of Re. The procedure is repeated till the two (or four) values of Re coincide. The weak dependence of both σ_r and σ_i on B is rather beneficial for the measurements, since the unavoidable gravitational field will not alter the results significantly. In other words, the plots of σ_r and σ_i *vs.* B will not be used to measure either viscosity or surface tension, rather they will be used to adjust values of σ_r and σ_i properly.

6.3. *Non-axisymmetric disturbances in zero gravity* ($k \neq 0, B = 0$)

Since $B = 0$ the static shape is again a cylinder. Non-axisymmetric modes have been experimentally observed by both Fowle *et al.* (1979) and Sanz & Diez (1989).

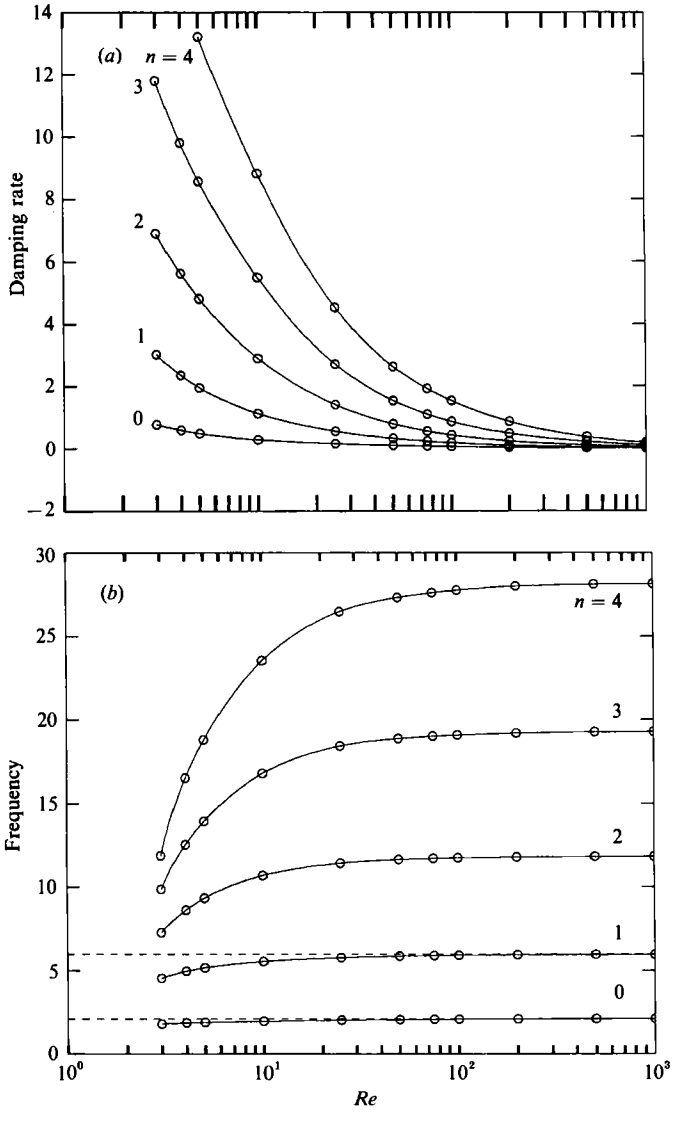

FIGURE 16. (*a*) Damping rate and (*b*) frequency of the first five non-axisymmetric modes as a function of Reynolds number for $\Lambda = 2$, $k = 1$. Open circles indicate numerical results of this work, dashed lines indicate results by Sanz & Diez (1989).

Azimuthal variations are described by the wavenumber k. The lowest mode that arises now has a plane of symmetry at $z = 0$, but it does not correspond to any mode presented earlier. Shapes of liquid bridges in this mode resemble one half of a sine wave (see figure 10). For this reason, Fowle *et al.* called it the 'C' mode; in the present work it is identified by $n = 0$. This mode is not allowed with axisymmetric disturbances because it would not conserve the volume of the liquid in the bridge. Each higher mode corresponds to one already presented for $k = 0$. Cross-sections of modes at the $(\theta = 0, \theta = \pi)$-plane and for $n = 1, 2, 3$ are shown in figure 10.

Both the damping rate and the frequency are seen to increase with the azimuthal wavenumber in figure 11. This effect is similar to increasing n and is because more

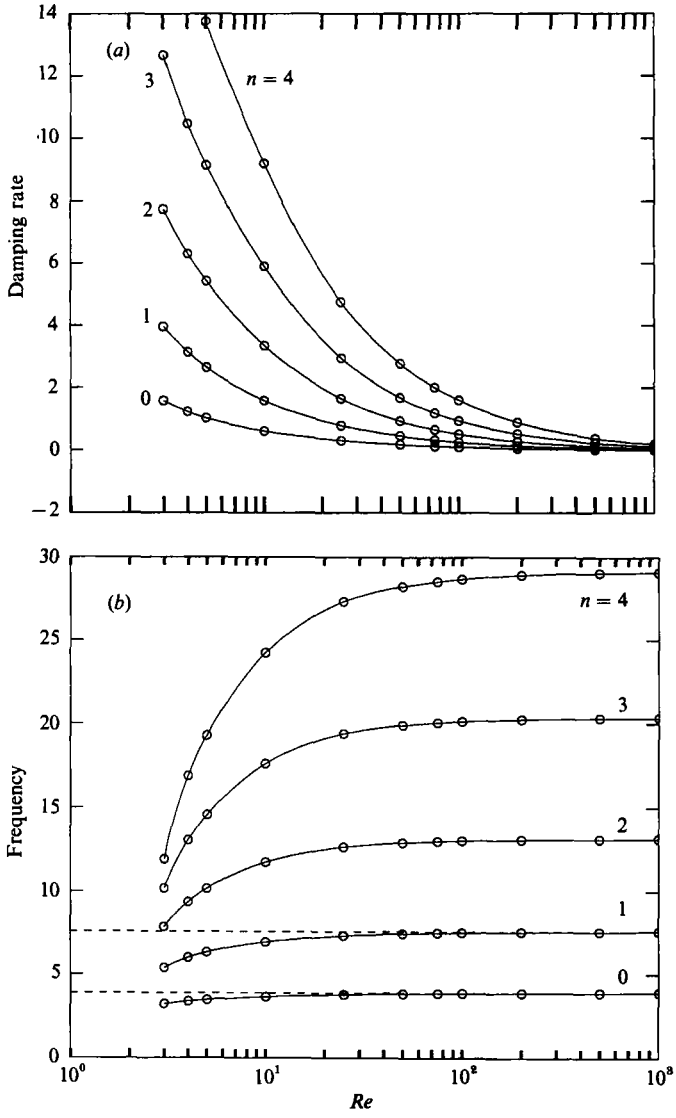

FIGURE 17. As figure 16 but for $k = 2$.

complex flow patterns dissipate energy more efficiently (i.e. higher σ_r) and are more difficult to excite (i.e. higher σ_i). When $k = 0$ results from the axisymmetric analysis are reproduced.

The dependence of the eigenvalues on aspect ratio for $Re = 10$ is shown in figures 12 and 13 for $k = 1$ and 2, respectively. The same dependence, but for $Re = 1000$, is shown in figures 14 and 15. Earlier observations and explanations are valid here as well. For example, eigenvalues monotonically increase with Λ, n and k. Calculated frequencies at large Re agree very well with those reported by Sanz & Diez, but their analysis cannot predict damping rates. Moreover, the bridge remains stable to dynamic and non-axisymmetric disturbances, even if Λ is decreased below the Rayleigh limit ($\Lambda = 0.5$). Thus, σ_r remains positive irrespective of the values of k and

Re. This is in accordance with the well-known results by Rayleigh (1879) and the more recent analysis of Preziosi *et al.* (1989).

Finally, the effect of *Re* for $\Lambda = 2$ is shown in figures 16 and 17 for $k = 1$ and 2, respectively. The stabilizing influence of larger azimuthal wavenumbers prevails throughout the study. Results from inviscid analysis (Sanz & Diez) are approached asymptotically as *Re* increases. Numerical values for non-axisymmetric oscillations and further results are given in Chen (1991).

7. Conclusions

Analytical and numerical methods have been used in order to determine the eigenvalues and eigenmodes of viscous oscillations of capillary bridges. Gravitational effects as well as axisymmetric and three-dimensional disturbances have been studied. It was found that both the damping rate and frequency of oscillation increases with the axial wavenumber (n), the azimuthal wavenumber (k), and the aspect ratio (Λ), and an explanation was given. Results obtained from inviscid and boundary-layer analyses have been confirmed and the range of their validity in terms of *Re* has been found. In small bridges ($\tilde{R} = \tilde{L} = 0.5$ cm) gravity does not modify the eigenvalues significantly, although static and dynamic shapes appear quite distorted. In spite of the fact that higher modes ($k \neq 0, n > 1$) have been experimentally excited, lower modes would provide important physical data more readily.

Usage of the Cornell National Supercomputer Facilities (CNSF) is gratefully acknowledged.

REFERENCES

Basaran, O. A., Scott, T. C. & Byers, C. H. 1989 Drop oscillations in liquid–liquid systems. *AIChE J.* **35**, 1263–1270.

Batchelor, G. K. 1967 *An Introduction to Fluid Dynamics*. Cambridge University Press.

Benjamin, T. B. & Scott, J. C. 1979 Gravity–capillary waves with edge constraints. *J. Fluid Mech.* **92**, 241–267.

Borkar, A. 1989 The dynamics of axisymmetric capillary bridges. M.S. thesis, Department of Chemical Engineering, SUNY at Buffalo, New York.

Borkar, A. & Tsamopoulos, J. A. 1991 Boundary-layer analysis of the dynamics of axisymmetric capillary bridges. *Phys. Fluids* A **3**, 2866–2874.

Brown, R. 1988 Theory of transport processes in single crystal growth from the melt. *AIChE J.* **34**, 881–911.

Chandrasekhar, S. 1959 The oscillations of a viscous liquid globe. *Proc. Lond. Math. Soc.* **9**, 141–149.

Chen, T.-Y. 1991 Static and dynamic analysis of capillary bridges. Ph.D. thesis, Department of Chemical Engineering, State University of New York at Buffalo, Buffalo, New York.

Coriell, S. R., Hardy, S. C. & Cordes, M. R. 1977 Stability of liquid zones. *J. Colloid Interface Sci.* **60**, 126–136.

Finucane, J. S. & Olander, D. R. 1969 The viscosity of uranium and two uranium–chromium alloys. *High Temp. Sci.* **1**, 466–480.

Fowle, A. A., Wang, C. A. & Strong, P. F. 1979 Experiments on the stability of conical and cylindrical liquid columns at low Bond numbers. *Arthur D. Little, Ref.* C-82435.

Joseph, D. D., Sturges, L. D. & Warner, W. H. 1982 Convergence of biorthogonal series of biharmonic eigenfunctions by the method of Titchmarsh. *Arch. Rat. Mech. Anal.* **78**, 223–274.

Lihrmann, J. M. & Haggerty, J. S. 1985 Surface tensions of alumina-containing liquids. *J. Am. Ceram. Soc.* **68**, 81–85.

MILLER, C. A. & SCRIVEN, L. E. 1968 The oscillations of a fluid droplet immersed in another fluid. *J. Fluid Mech.* **32**, 417–435.

PADDAY, J. F. 1971 The profiles of axially symmetric menisci. *Phil. Trans. R. Soc. Lond.* A **269**, 265–293.

PLATEAU, J. A. F. 1863 Experimental and theoretical researches on the figures of equilibrium of a liquid mass withdrawn from the action of gravity. Translated in *Ann. Rep. Smithsonian Institution*, pp. 207–285.

PREZIOSI, L., CHEN, K. & JOSEPH, D. D. 1989 Lubricated pipelining: Stability of core–annular flow. *J. Fluid Mech.* **201**, 323–356.

PROSPERETTI, A. 1980 Normal-mode analysis for the oscillations of a viscous liquid drop in an immiscible liquid. *J. Méc.* **19**, 149–182.

RAYLEIGH, LORD 1879 On the instability of jets. *Proc. Lond. Math. Soc.* **10**, 4–13.

RUSSO, M. J. & STEEN, P. H. 1986 Instability of rotund capillary bridges to general disturbances: Experiment and theory. *J. Colloid Interface Sci.* **113**, 154–163.

SANZ, A. 1985 The influence of the outer bath in the dynamics of axisymmetric liquid bridges. *J. Fluid Mech.* **156**, 101–140.

SANZ, A. & DIEZ, J. L. 1989 Non-axisymmetric oscillation of liquid bridges. *J. Fluid Mech.* **205**, 503–521.

SMITH, R. C. T. 1952 The bending of a semi-infinite strip. *Austral. J. Sci. Res.* A **5**, 227–237.

STRANI, M. & SABETTA, F. 1988 Viscous oscillations of a supported drop in an immiscible fluid. *J. Fluid Mech.* **189**, 397–421.

THOMAS, P. D. & BROWN, R. A. 1987 LU decomposition of matrices with augmented dense constraints. *Intl J. Numer. Meth. Engng* **24**, 1451–1459.

TRINH, E. H., MARSTON, P. L. & ROBEY, J. L. 1988 Acoustic measurement of the surface tension of levitated drops. *J. Colloid Interface Sci.* **124**, 95–103.

TRINH, E., ZWERN, A. & WANG, T. G. 1982 An experimental study of small-amplitude drop oscillations in immiscible liquid systems. *J. Fluid Mech.* **115**, 453–474.

TSAMOPOULOS, J. A. & BROWN, R. A. 1983 Nonlinear oscillations of inviscid drops and bubbles. *J. Fluid Mech.* **127**, 519–537.

TSAMOPOULOS, J. A., POSLINSKI, A. J. & RYAN, M. E. 1988 Equilibrium shapes and stability of captive annular menisci. *J. Fluid Mech.* **197**, 523–549.

YOO, J. Y. & JOSEPH, D. D. 1978 Stokes flow in a trench between concentric cylinders. *SIAM J. Appl. Maths.* **34**, 247–285.

ZHANG, Y. & ALEXANDER, J. 1990 Sensitivity of liquid bridges subject to axial residual acceleration. *Phys. Fluids* A **2**, 1966–1974.